Variability of sun-induced chlorophyll fluorescence according to stand age-related processes in a managed loblolly pine forest

ROBERTO COLOMBO[1], MARCO CELESTI[1], REMO BIANCHI[2], PETYA K. E. CAMPBELL[3], SERGIO COGLIATI[1], BRUCE D. COOK[4], LAWRENCE A. CORP[5], ALEXANDER DAMM[6], JEAN-CHRISTOPHE DOMEC[7,8], LUIS GUANTER[9], TOMMASO JULITTA[1], ELIZABETH M. MIDDLETON[4], ASKO NOORMETS[10], CINZIA PANIGADA[1], FRANCISCO PINTO[11,12], UWE RASCHER[11], MICOL ROSSINI[1], ANKE SCHICKLING[11]

[1]*Remote Sensing of Environmental Dynamics Lab., DISAT, Università di Milano-Bicocca, P.zza della Scienza 1, 20126 Milan, Italy;* [2]*ESA-ESRIN Earth Observations, 00044 Frascati, Italy,* [3]*Joint Center for Earth Systems Technology, University of Maryland Baltimore County, Baltimore, MD, USA;* [4]*Biospheric Sciences Laboratory, NASA/GSFC, Greenbelt, MD 20771, USA;* [5]*Science Systems & Applications Inc., Lanham, MD, USA;* [6]*Remote Sensing Laboratories, University of Zurich, Zurich, Switzerland;* [7]*Bordeaux Sciences Agro, UMR 1391 INRA-ISPA, 33175 Gradignan Cedex, France;* [8]*Nicholas School of the Environment, Duke University, Durham, NC 27708, USA;* [9]*Helmholtz Centre Potsdam, German Research Center for Geosciences (GFZ), Germany;* [10]*Dept. Forestry & Environmental Resources, North Carolina State University, Raleigh, NC, USA;* [11]*Institute of Bio and Geosciences, IBG-2: Plant Sciences, Forschungszentrum Jülich GmbH, 52425 Jülich, Germany;* [12]*Global Wheat Program, International Maize and Wheat Improvement Center (CIMMYT), Mexico.*

Abstract

Leaf fluorescence can be used to track plant development and stress, and is considered the most direct measurement of photosynthetic activity available from remote sensing techniques. Red and far-red Sun Induced chlorophyll Fluorescence (SIF) maps were generated from high spatial resolution images collected with the *HyPlant* airborne spectrometer over even-aged loblolly pine plantations in North Carolina (USA). Canopy fluorescence yield (i.e., the fluorescence flux normalized by the light absorbed) in the red and far-red peaks was computed. This quantifies the fluorescence emission efficiencies that is more directly linked to canopy function compared to SIF radiances. Fluorescence fluxes and yields were investigated in relation to tree age to infer new insights on the potential of those measurements in better describing ecosystem processes. The results showed that red fluorescence yield varies with stand age. Young stands exhibited a nearly 2-fold higher red fluorescence yield than mature forest plantations, while the far-red fluorescence yield remained constant. We interpreted this finding in a context of photosynthetic stomatal limitation in aging loblolly pine stands.

Current and future satellite missions provide global datasets of SIF at coarse spatial resolution, resulting in intra-pixel mixture effects, which could be a confounding factor for fluorescence signal interpretation. To mitigate this effect, we propose a surrogate of the fluorescence yield, namely the Canopy Cover Fluorescence Index (CCFI) that accounts for the spatial variability in canopy structure by exploiting the vegetation fractional cover. It was found that spatial aggregation tended to mask the effective relationships, while the CCFI was still able to maintain this link.

This study is a first attempt in interpreting the fluorescence variability in aging forest stands and it may open new perspectives in understanding long-term forest dynamics in response to future climatic conditions from remote sensing of SIF.

Introduction

Leaf structure and physiology change in many woody species when they become sexually mature (e.g., Greenwood, 1995). Compared with the knowledge of senescence processes in annuals and biennial plants, relatively little is known about age-related changes in woody perennials (Bond, 2000). Old trees differ from younger trees, both physiologically and morphologically. In general, older trees have lower rates of photosynthesis, reduced growth rates (both height and diameter) and a distinctive hydraulic architecture (Ryan & Yoder, 1997; Meinzer *et al*., 2011). Nutrition, carbon allocation (including respiration), meristematic activity and the tree's hydraulic properties all potentially change with tree age and in most cases result in a slower growth in older trees (Domec & Gartner, 2003). Moreover, it is generally known that photosynthetic rates of seedlings are higher than in mature trees (Larcher, 1969). Leaf photosynthesis and stand primary production have often been found to decline with increasing plant age and size, as a result of hydraulic or biochemical limitations (Yoder *et al*., 1994; Hubbard *et al*., 1999; Ryan *et al*., 2006; Drake *et al*., 2011). Determining why growth is reduced in aging forest stands is a compelling need: the growth patterns are pronounced and predictable but the underlying mechanisms remain unclear (Gower *et al*., 1996; Ryan *et al*., 1996). Even though some work has been done at the leaf level (Shirke, 2001; Reinhardt *et al*., 2009; de Beek *et al*, 2010; Linkosalo *et al*., 2014), the response of Sun-Induced chlorophyll Fluorescence (SIF) to these age-related processes has not been investigated previously. SIF is closely related to actual photosynthetic rates and basically to the functional process linked to the amount of energy (in form of transported electrons) that is provided from photosynthetic light reactions (Porcar-Castell *et al*., 2014).

Remote sensing of SIF is a research field of growing interest with the potential to provide an improved tool for monitoring plant status and photosynthetic function from above. In this

69 framework, the new satellite mission of the European Space Agency, the FLuorescence

70 EXplorer (FLEX; Drusch *et al*., 2017), is expected to map canopy fluorescence from space at

71 global level, with 300 m spatial resolution, which will be used to derive the photosynthetic

72 activity of natural and managed ecosystems. Fluorescence is considered the most direct proxy

73 of actual photosynthetic activity available from remote sensing techniques and as such it has

74 been used extensively to track plant status at leaf and canopy level (Moya *et al*., 2004; Meroni

75 *et al*., 2006, 2008; Rascher *et al*., 2009; Damm *et al*., 2010; Daumard *et al*., 2010; Rossini *et*

76 *al*., 2010; Middleton *et al*., 2012; Zarco-Tejada *et al*., 2012; Cheng *et al*., 2013; Joiner *et al*.,

77 2014; Zhang *et al*., 2014; Ac *et al*., 2015; Koffi *et al*., 2015; Rossini *et al*., 2015; Zarco-Tejada

78 *et al*., 2016; Goulas *et al*., 2017).

79 The intensity of the fluorescence signal at canopy level depends on the photosynthetic rates,

80 biophysical, biochemical and structural characteristics of the canopy, incoming radiation and

81 background contributions (Hoge *et al*., 1983; Olioso *et al*., 1992; Cerovic *et al*., 1996; Moya *et*

82 *al*., 2006; Daumard *et al*., 2010; Fournier *et al*., 2012; Van Wittenberghe *et al*., 2013; Damm *et*

83 *al*., 2015a, 2015b; Verrelst *et al*., 2015; Rossini *et al*., 2016). These parameters are highly

84 variable in space and time and they should all be considered to correctly interpret the

85 fluorescence signal. In fact, plants with different photosynthetic rates, chlorophyll content

86 and/or canopy structure and exposed to various irradiance regimes can potentially emit the same

87 amount of fluorescence. The effects of variable incoming illumination can be corrected by

88 computing the *apparent* fluorescence yield (i.e., the ratio of the emitted fluorescence flux to the

89 total incoming Photosynthetically Active Radiation (PAR), which is in fact the parameter most

90 commonly exploited for spatial and temporal comparison of fluorescence satellite derived

91 products collected in different light illumination conditions (i.e., different solar zenith angles,

92 e.g., Guanter *et al*., 2014). However, to move towards the use of SIF for net photosynthesis and

93   plant functioning characterization in a heterogeneous landscape, it is also necessary to account

94   for vegetation structural/biochemical variations. This can be accomplished by exploiting the

95   *true* canopy fluorescence yield (ε_f; i.e., the ratio of the emitted fluorescence flux to the

96   Absorbed Photosyntetically Active Radiation, APAR), which is a physically-based index of

97   efficiency that accurately describes the effects of the absorbed radiation on the SIF signal. The

98   usefulness of fluorescence or the apparent fluorescence yield to track the effects of

99   environmental stressors on plant functioning has been demonstrated in numerous investigations

100   (e.g., Meroni et al., 2008; Guanter et al., 2014), while the performances of the true fluorescence

101   yield computed at airborne or satellite level has been investigated in only two studies (Sun *et*

102   *al*., 2015; Wieneke *et al*., 2016;). This is mainly due to the difficulty in accurately estimating

103   APAR, which is challenging.

104   Current and future satellite missions will provide global datasets of fluorescence at a range of

105   coarse spatial resolutions (e.g., 300 m to 0.5º), resulting in intra-pixel mixture effects, which

106   will be an unavoidable confounding factor for fluorescence signal interpretation. In this context,

107   there is a need of having simplified fluorescence indices for small-scale applications over large

108   regions, which can take into account the spatial variability of canopy structure. Therefore, a

109   new approach is needed to compensate for structural effects on SIF measurements, including

110   the use of radiative transfer model inversion (van der Tol *et al*., 2016; Hernández-Clemente *et*

111   *al*., 2017; Zhao et al., 2016), spectrally invariant correction factors (e.g., the Directional Area

112   Scattering Factor, Knyazikhin *et al*., 2012), or empirical normalization techniques (Colombo *et*

113   *al*., 2016).

114   In this paper, red and far-red SIF maps were generated from high spatial resolution images (1

115   m) collected with the *HyPlant* airborne sensor over a range of even aged stands in loblolly pine

116   forest plantations in North Carolina (USA). The true canopy fluorescence yields for both red

117 and far-red SIF were then computed and investigated with the main aim to understand if

118 fluorescence varies across stands of different ages, according structural and physiological

119 parameters. In this context, we hypothesized that hydraulic limitation in older pines could

120 reflect in a lower fluorescence emission compared to the younger trees, due to the reduced rates

121 of photosynthesis. We were also interested in evaluating the effect of pixel size and the mixture

122 effects on the relationships between fluorescence and stand age. This study can be considered

123 a first attempt in interpreting the fluorescence variability in aging forest stands and it may open

124 new perspectives in understanding long-term forest dynamics from remote sensing of SIF.

125

126 **Data and methods**

127 *Study area*

128 This study was performed at the Parker Tract forest in the lower coastal plain near Plymouth,

129 North Carolina, USA, in the context of the joint 2013 ESA/NASA FLEX airborne campaign

130 (Middleton *et al*., 2017). The forest is a 4,400 ha managed plantation that contains various

131 loblolly Pine (*Pinus taeda* L.) stands of different ages. Parker Tract is a pine forest where stand

132 density is reduced under a prescribed thinning regime as age increases to maximize timber

133 production. According to the Parker Tract forest management plan, pine stand age within the

134 study area ranged from 3 to 46 years old, when the forests have reached high commercial

135 potential and are being harvested. Therefore, we are dealing with juvenile and mature stages.

136 The topography is flat and the climate is maritime temperate zone with a mean annual

137 precipitation of 1320 mm and mean annual temperature of 15.5 °C. The Parker Tract forest

138 belongs to the Long-Term Ecological Research Sites and further details on the site are reported

139 in different studies (e.g., Noormets *et al*., 2010; Domec *et al*., 2012). Figure 1 shows the location

140 of the study area and the investigated loblolly pine stands (with their plantation age) overlapped

141 to the *HyPlant* mosaic of airborne images collected over the investigated forest.
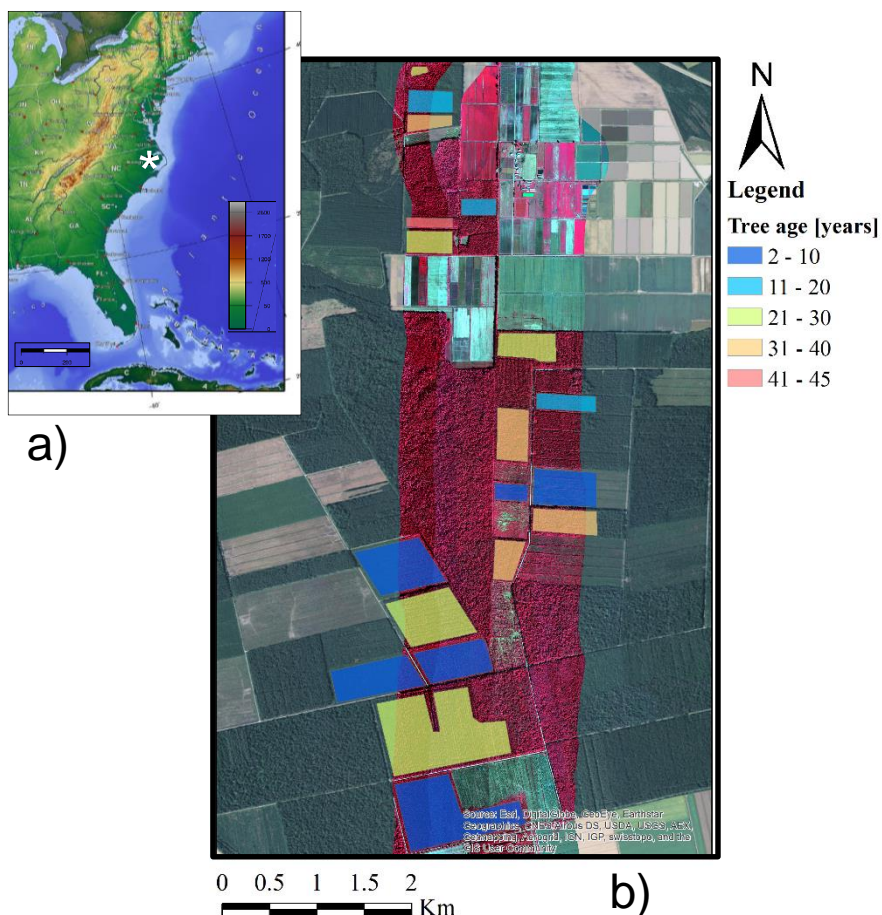
142

143 **Fig. 1** a) Location of the Parker Tract Forest in NC, USA; b) Location of the loblolly pine even-

144 aged stands (18 total) are shown in colored categories, overlapped on a false color composite

145 *HyPlant* mosaic.

146

147 The tree age classes reported in Figure 1 correspond to years since planting at the time of data

148 acquisition. In particular, tree ages correspond to the time when the sites were graded and

149 planted with 2-year-old seedlings, and thus can be considered a chronosequence.

150 Since no direct dendrochonological and only few physiological measurements were available

151 for comparison between forest data and fluorescence estimates, to better interpret our findings

152 we also exploited data and previous results obtained in a companion loblolly forest at the Duke

153 Forest. The Duke Forest loblolly study area is located in the Blackwood Division of Duke Forest

154 (US-Dk3; lat/lon 35.97816586/-79.09419556, North Carolina, USA). It represents a late stage

155 post-agricultural succession characteristic of the south-eastern United States. Duke Forest, in

156 addition to mixed deciduous forest, also has even-aged plantation of loblolly pine stands

157 ranging from 14 to 114 years, established in 1983 following a clear cut and a burn (Oren *et al*.,

158 2006; Novick *et al*., 2009; Domec *et al*., 2015).

159

160 *Field campaign and leaf level measurements*

161 During the field survey in September and October 2013, forest stand characteristics including

162 average tree height, crown width, crown depth, and tree diameter at breast height (1.3 m) were

163 measured within one-tenth of an acre (0.4 ha) plots and averaging measurements from 2-3 plots

164 per stand, at both Parker Tract (18 stands) and Duke Forest (14 stands). Leaf area index (LAI)

165 was measured at all stands using a LAI-2000 Plant Canopy Analyzer (LAI-2000 PCA; Li-Cor,

166 Lincoln, NE, USA). LAI measurements at each location were taken using a standard protocol

167 in diffuse light conditions within one hour of dawn or dusk.

168 Average carbon (%C) and nitrogen concentration (%N) for pine foliar samples were measured

169 in 26 stands (18 at Duke Forest and 8 at Parker Tract), while leaf chlorophyll content was

170 estimated at 16 stands in Parker Tract. Leaf samples were collected from the 2 most recent

171 annual leaf flushes on 1-3 branches of the sunlit portion of the upper canopy from 3 pine trees

172 in a stand, using a cherry picker or a rifle. The branch samples were placed in a bag with wet

173   paper towel, on ice, in a dark cooler and taken to a nearby field lab for analysis. Leaf fresh and

174   dry weights were measured on 10 needle fascicles from a sample, using three samples per tree.

175   For pigment determination, needle samples were ground and placed in polystyrene cuvettes

176   containing 4 mL dimethyl sulfoxide (DMSO) and frozen for extraction before the

177   measurements. A spectrophotometer was used to determine chlorophyll *a*, chlorophyll *b*, total

178   chlorophyll (Cab, mg/cm^2), and carotenoids based on established equations (Chapelle and Kim,

179   1992).

180   Leaf reflectance and transmittance spectra were also measured on needles collected from 25

181   trees (1-2 trees per stand at Parker Tract), at the end of the growing season, when the needles

182   were fully developed. Hemispherical reflectance and transmittance were measured using an

183   ASD spectrometer (FieldSpec 3, Analytical Spectral Devices, Inc., Bolder Co.) equipped with

184   an external integrating sphere (LI-1800, Li-Cor, Lincoln, NE, USA) and then used to determine

185   fraction of APAR (fAPAR) at leaf level.

186   Stomatal conductance (g_s) and net photosynthesis (P_{net}) measurements at the Parker Tract forest

187   were performed in 2013 on May 17th, and September 30th for the mature pine trees (23 years

188   old trees) and on June 2nd and October 1st for the young trees (7 years old trees). Meteorological

189   conditions were stable during those weeks and were characterized by clear and warm days.

190   Stomatal conductance and photosynthesis were measured with a LI-6400 gas exchange system

191   (LI-COR, Lincoln, NE, USA). Measurements of g_s were performed on six randomly selected

192   individuals within each age class every two hours beginning at 06:00 h solar time and ending

193   at approximately 15:00 h solar time. Measurements of g_s were conducted on current-year

194   detached fascicles taken from the same shoot simultaneously, and were performed on fully sun

195   exposed south-facing shoots. For the mature trees, shoots from the upper canopy were shot

196   down with a rifle. Needles were not detached for more than five minutes before the

197   measurements were initiated. Previous studies on the same tree species have shown that there

198   were no differences between excised and attached needle gas exchange when measurements

199   were restricted to less than 15 min after excision (Maier *et al.,* 2008; Drake et *al*., 2010). For

200   each needle, the chamber was set to match prevailing environmental conditions assessed

201   immediately prior to the measurement: atmospheric CO_2 concentration (384-405 ppm), relative

202   humidity (46-61 %), photosynthetically active radiation (600-1800 μmol m^{-2} s^{-1}), and leaf

203   temperature (27-35 °C). Stomatal conductance and photosynthesis data reported here

204   correspond to the maximum values, i.e., usually taken between 09:30 h and 11:30 h solar time.

205   For normalizing g_s on an all-sided leaf area basis, needle areas were obtained geometrically

206   from dimensions measured using a digital caliper (series 500 Mitutoyo, Aurora, IL, USA)

207   (Rundel & Yoder 1998). Along with the gas exchange measurements, leaf water potential (Ψ_{leaf})

208   were measured at predawn and at midday (11:00 h-12:00 h solar time) using a pressure chamber

209   (PMS Ins., Albany, OR, USA). For the midday measurements, Ψ_{leaf}, g_s and P_{net} were conducted

210   on detached fascicles taken from the same shoot.

211

212   *Airborne acquisition and pre-processing*

213   On October 26th 2013, from 09:56 h to 11:08 h solar time, eight aerial images were acquired by

214   the *HyPlant* airborne imaging spectrometer on board the NASA Langley Research Center's

215   (LARC) UC12 Beechcraft King Air in combination with imagery acquired by the Goddard

216   LiDAR, Hyperspectral and Thermal (G-LiHT) Airborne system. Extensive descriptions of

217   these systems are presented in Rascher *et al*., (2015), Cook *et al*., (2013) and Middleton *et al*.,

218   (2017).

219   The *HyPlant* instantaneous field of view (IFOV) is equal to 0.0832°, while the FOV is of 32.3°.

220   With such a configuration, the aircraft was flown at an average altitude of 610 m, resulting in a

221   *HyPlant* swath of 384 m, with a spatial pixel size of 1 m. *HyPlant* system consists of two

222   modules: the broad band dual-channel module (DUAL) to compute surface reflectance in the

223   visible through near and short wave infrared spectral region (380-2500 nm) and the fluorescence

224   module (FLUO) which operates at higher spectral resolution in the 670-780 nm spectral range

225   designed for fluorescence retrievals. *HyPlant* at-sensor radiance images from the FLUO and the

226   DUAL modules were generated through a dedicated processing chain. The Atmospheric &

227   Topographic Correction model (ATCOR, ReSe Applications Schläpfer) was run to perform the

228   atmospheric correction and then all the images were georectified using the CaliGeo toolbox

229   (SPECIM, Finland). In addition to reflectance and fluorescence, spectral vegetation indices

230   were generated using the *Hyplant* data. An example of radiance measurements from a loblolly

231   pine acquired with the FLUO module is shown in Figure 2.

232
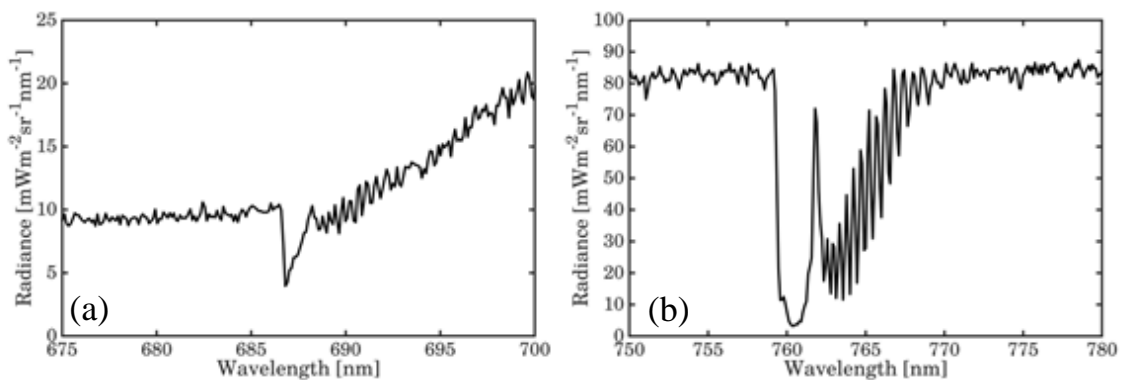
233   **Fig. 2** Example of the spectral radiance extracted from the *HyPlant* image (FLUO module) for

234   a loblolly pine around oxygen B (a) and A (b) absorption bands.

235

236   A canopy tree height map was obtained from the LiDAR data. Classification of G-LiHT LiDAR

237   ground   returns   was   performed   with   a   progressive   morphological   filter   with   Delaunay

238 triangulation to generate a Triangulated Irregular Network (TIN) of ground hits, and the TIN

239 was then used to linearly interpolate the Digital Terrain Model on a 1 m raster grid.

240 Additionally, the TIN was used to interpolate the base elevation of every non-ground return,

241 and vegetation heights were computed by difference. The Canopy Height Model (CHM) was

242 created by selecting the greatest return height in every 1 m grid cell. Tree height, defined as the

243 maximum height of each tree, was derived from the CHM by finding the local maximum in a

244 moving window of 3x3 pixels (3x3 m). Local maxima lower than the 1st quartile of the CHM

245 in the stand were not considered representative of a tree, thus they were neglected. The average

246 tree height for each stand was computed as the average of all tree heights (i.e., the local maxima)

247 within each stand.

248

249 *Retrieval of Sun-Induced Fluorescence*

250 Among different approaches available for the retrieval of SIF (e.g., Cogliati *et al*., 2015), the

251 Singular Vector Decomposition (SVD) (Guanter *et al*., 2012; 2013) was selected for this study

252 based on successful results with *Hyplant* data in other studies (e.g., Rossini *et al*., 2015). This

253 data-driven approach relies on two key assumptions: *i*) a given radiance spectrum can be

254 modelled as the linear combination of a reflected surface radiance plus a SIF emission

255 propagated to at-sensor level, and *ii*) the reflected surface radiance can be formulated as a linear

256 combination of orthogonal spectral vectors. The SVD is comparable to a principal component

257 analysis and reduces the dimensionality of a large set of correlated variables (e.g., training

258 radiance spectra that are free of SIF emissions) by transforming it into a small set of

259 uncorrelated variables (singular vectors).

260   The definition of a forward model (F) to describe a measured radiance signal including SIF

261   emissions at sensor level comprises several spectral functions (singular vectors) representing

262   the signal intensity due to surface albedo, illumination angle, atmospheric absorption and

263   scattering effects, spectral slope as a function of surface reflectance, and sensor effects (spectral

264   shifts, band broadening). Further, SIF radiance ($Wm^{-2}sr^{-1}nm^{-1}$) is considered as an additive

265   component to complement the forward model as:

266    $$F(\omega, SIF) = \sum_{i=1}^{n_v} \omega_i v_i + SIF, \qquad\qquad (1)$$

267   where ω_i corresponds to the weight of a particular singular vector v_i. Typically, 4-5 singular

268   vectors are used to model the at-sensor radiance signal, considering an empirical threshold of

269   0.05% as minimum information content of a singular vector.

270   Few adjustments were applied to improve the inversion results, such as removing the strongest

271   absorption features since the forward model does not include any physical formulation of

272   atmospheric absorption or scattering effects, nor the normalization of input radiances and

273   radiances used to obtain the singular vectors based on their spectral slope.

274   The inversion of F was done by means of standard least squares fitting using a retrieval error

275   covariance S_e that is given as:

276    $$S_e = \delta_m^2 (J^T J)^{-1}, \qquad\qquad (2)$$

277   where δ_m is the measurement error approximated as standard deviation of a subset of used

278   reference radiance signals and J is the matrix containing the singular vectors and J^T is its

279   transpose.

280   The SVD algorithm was applied to the *HyPlant* FLUO data to produce maps for the canopy red

281   SIF radiances at 690 nm and far-red SIF 740 nm radiances at the full native *HyPlant* spatial

282   resolution (1 m).

283
284   *Retrieval of Absorbed Photosynthetic Active Radiation*

285   The APAR maps were computed as the product of fAPAR and the incoming PAR values.

286   fAPAR can be derived from remote sensing, exploiting either physically based or empirical

287   strategies using spectral vegetation indices (e.g., Walter-Shea *et al*., 1997; Myneni *et al*. 2002;

288   Gobron *et al*., 2006; Donohue *et al*., 2008; Widlowski, 2010; D'Odorico *et al*., 2014; Pickett-

289   Heaps *et al*., 2014). Following a scheme analogous to Damm *et al*., (2010), but using the

290   spectral reflectance instead of the incident and reflected radiance, fAPAR was computed in this

291   study as (1-reflectance) in the PAR region (400-700 nm). In addition, for comparison purposes,

292   we also estimated fAPAR as a linear model of Normalized Difference Vegetation Index (NDVI)

293   (Hatfield *et al*., 1984; Goward & Huemmrich, 1992; Myneni & Williams, 1994; Liu *et al*.,

294   2017).

295   The incident PAR was measured at the US-NC2 loblolly plantation flux tower at half-hourly

296   steps, and interpolated to actual overflight times with a piecewise polynomial smoothing spline.

297   During the overpasses (i.e., between 09:56 h and 11:08 h solar time), PAR varied between 1130

298   μmol m^{-2} s^{-1} and 1430 μmol m^{-2} s^{-1} (247 to 313 W m^{-2}).

299

300

Computation of true fluorescence yields of loblolly pine

302 The SIF flux can be modelled as the product of PAR, fAPAR and ε_f. The last term is the amount

303 of absorbed radiation emitted as fluorescence, and is referred to here as canopy-level "true

304 fluorescence yield" (e.g., Lee *et al.*, 2013):

305 $$SIF_{[\lambda,t]} = \varepsilon_{f[\lambda,t]} \cdot PAR_{[400\text{-}700,t]} \cdot fAPAR_{[t]}$$ (3)

306 The fluorescence flux is dependent on wavelength (λ) and time (t) at which the flux is emitted.

307 For full emission spectra, the entire wavelength range from 650 nm to 800 nm should be

308 considered. Canopy-level true fluorescence yield is related to leaf-level fluorescence yield,

309 neglecting a second-order term accounting for the reabsorption of the red fluorescence within

310 the canopy and the canopy anisotropy, at both red and far-red wavelengths (Guanter *et al.*, 2014;

311 Damm *et al.*, 2015b).

312 In this study, the computation of the SIF yields at full (1 m) spatial resolution was conducted

313 selecting only the loblolly SIF radiance in each stand. A supervised classification scheme based

314 on the *HyPlant* DUAL reflectance images was therefore implemented to identify loblolly pine

315 (mainly sunlit pixels). Two hundred training pixels were randomly selected and visually

316 assigned to one of the four spectrally distinguishable classes (i.e., loblolly pine, shadow, bare

317 soil, and other vegetation components). The classified map was used as a mask to extract SIF

318 and APAR of the loblolly component within 18 different stands identified as Regions of Interest

319 (ROI) of 84 x 84 pixels each. The dimension of the ROI was set according to the forest stand

320 dimensions to get an average stand values of red and far-red SIF and APAR for the loblolly

321 component (hereafter SIF_{lob}^{690}, SIF_{lob}^{740} and $APAR_{lob}$), and the corresponding true fluorescence

322 yields (hereafter ϵ_{lob}^{690} and ϵ_{lob}^{740}). The subscript *lob* indicates the loblolly pine class. The ROIs

323   were selected as close to nadir as possible in order to minimize possible effects dependent on

324   airborne cross-track viewing angles.

325   The true fluorescence yield maps of the loblolly component were then obtained using Equations

326   4 and 5, based on values from the maps of loblolly SIF and APAR.

327     $$\varepsilon_{lob}^{690} = \frac{SIF_{lob}^{690}}{APAR_{lob}} \qquad (4)$$

328     $$\varepsilon_{lob}^{740} = \frac{SIF_{lob}^{740}}{APAR_{lob}} \qquad (5)$$

329   where $APAR_{lob}$ is the product of PAR and fAPAR maps of the loblolly pine obtained with the

330   different overpasses. We also tested the apparent fluorescent yield, usually employed in remote

331   sensing of fluorescence studies when information about APAR is not available.

332

333   *Spatial aggregation and definition of the Canopy Cover Fluorescence Index*

334   In the analysis at full resolution, the scheme used in this study was similar to that suggested by

335   Zarco-Tejada *et al*., (2004) and Malenovsky *et al*., (2013), so that the SIF yields were mainly

336   extracted from sunlit pixels. The 1 m pixel size allowed the detection of pixels of homogenous

337   vegetation within the stands. *HyPlant* data were collected in October when the dominant green

338   land cover type was the loblolly pine. Other components, such as understory and deciduous

339   trees, were mainly displaying early autumn senescent foliage, while shadows and bare soils

340   were the most common classes in older and younger stands, respectively. In these forests, when

341   data are aggregated to even 10 m spatial resolution, these components become mixed and it

342   becomes difficult to find and isolate loblolly components.

343 To evaluate if the relationships between SIF and age-related processes are affected by pixel size

344 (surface heterogeneity), a simple spatial-aggregation analysis was carried out by resampling the

345 data at different spatial resolutions (i.e., pixel sizes of 10 x 10, 30 x 30, 60 x 60 and 84 x 84

346 pixels). The maximum aggregation was fixed at 84 x 84 pixels in order to be consistent with

347 the overall stand size, since larger aggregations would result in including trees with different

348 ages. The output of this process generated maps at different pixel (p) sizes, using aggregated

349 red and far-red fluorescence radiances (SIF_p^{690}, SIF_p^{740}), $APAR_p$, red-fluorescence and far-red

350 fluorescence yields ($\varepsilon_p^{690} = \frac{SIF_p^{690}}{APAR_p}$; $\varepsilon_p^{740} = \frac{SIF_p^{740}}{APAR_p}$).

351 We can reasonably assume that the fluorescence value of a generic pixel p can be expressed

352 with a linear mixing model driven by vegetation fractional cover (Zarco-Tejada *et al*., 2013;

353 Hernández-Clemente et al., 2017; ESA, 2017). In this study, the vegetation fractional cover of

354 the loblolly (fc_{lob}) was computed as the ratio between the number of pixels of the loblolly class

355 divided by total number of pixels in the ROI. For the case having only two components within

356 a pixel, the fluorescence flux of the aggregated pixel can be derived from the target component

357 (i.e., in this case the loblolly pine SIF, SIF_{lob}^{690}, SIF_{lob}^{740}), the fluorescence of the other

358 components (oc) within the pixel (SIF_{oc}^{690}, SIF_{oc}^{740}) and the fractional cover of the loblolly pine.

359 Therefore, the aggregated red SIF radiance can be estimated as follows:

360 $$SIF_p^{690} = SIF_{lob}^{690} \cdot fc_{lob} + SIF_{oc}^{690} \cdot (1 - fc_{lob}) \qquad\qquad (6)$$

361 The SIF_{oc}^{690} term in the study area is mainly a combination of senescent vegetation, bare soil

362 and shadows, and we can reasonably consider that such fluorescence flux is almost null or

363 negligible. The fluorescence flux of the loblolly component can be therefore directly derived

364 by the knowledge of the aggregated SIF value and its fractional cover. Using this scheme, we

365 can introduce the Canopy Cover Fluorescence Index (CCFI) that makes use of the loblolly cover

366 fraction within the pixel rather than the typically used fAPAR as the basis for normalizing the

367 SIF fluxes:

368 $$CCFI^{690} = \frac{SIF_p^{690}}{fc_{lob}}$$ (7)

369 This index is considered here to be independent from the spatial variability of land cover

370 proportions within each pixel. In other words, for a single vegetation class discontinuously

371 covering the soil surface the CCFI approximates ε_{lob}^{690}, allowing comparisons of fluorescence

372 across spatial scales without bias due to the different amounts of vegetation coverage in each

373 pixel.

374

375 *Statistical analysis*

376 The previously described fluorescence metrics were investigated across stands of different ages

377 with data aggregated to different spatial resolutions, by using regression models. Statistical

378 analysis and coding was performed in Matlab R2016a (MathWorks, USA) and IDL 8.2 (Exelis

379 VIS, USA), while image visualization and rendering was done in ENVI 5.2 (Exelis VIS, USA)

380 and QGIS 2.14 (Quantum GIS Development Team, 2016).

381

382 **Results**

383 *Spatial pattern of forest fluorescence*

384 An example of SIF maps for three loblolly pine stands characterized by different ages is shown

385 in Figure 3, with the RGB reflectance map from the *HyPlant* DUAL and the Canopy Height

386 Model derived from the G-LiHT LiDAR data. The different proportions of shadow and sunlit

canopy, as well as the spatial arrangement of the sunlit and shadowed components, are clearly

distinguishable in the three stands. In particular, in the younger stands the row-structured

pattern followed for plantation is clear, while in the oldest stand canopy closure obscures the

planting arrangement. Fluorescence maps show similar spatial patterns, with lower values in

bare or shadowed areas and higher values in the sunlit portion of the canopy. The inter-crown

gap pattern in the younger stands is clearly visible both in red and far-red SIF maps.
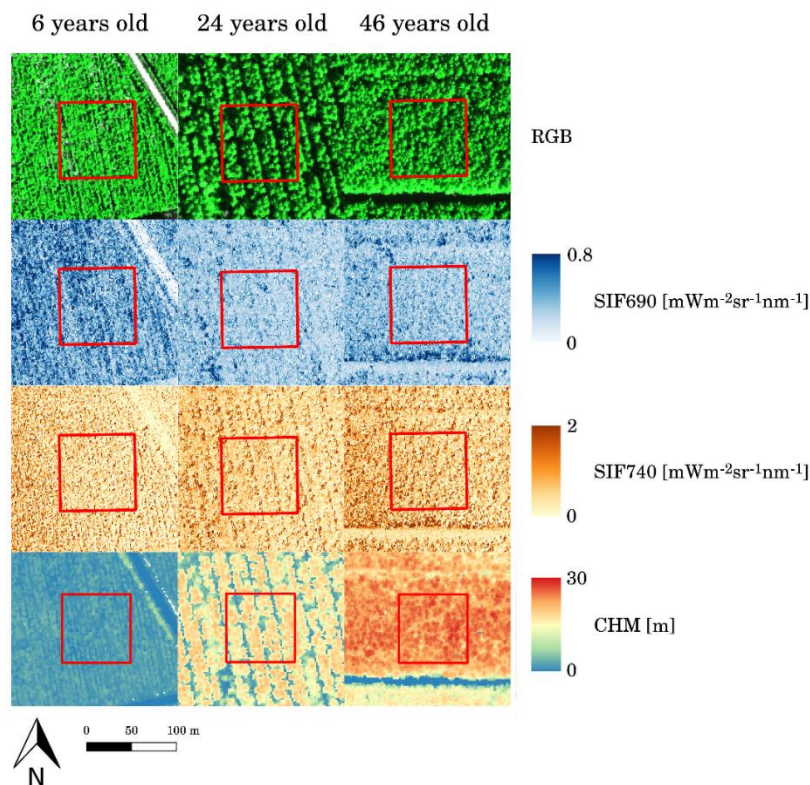
Fig. 3 Example of three loblolly pine stands characterized by different ages and heights (left to right: 6, 24 and 46 years old). From top to bottom: RGB color composite from the HyPlant DUAL, SIF at 690 nm and 740 nm from the HyPlant FLUO, and canopy height map from the G-LiHT LiDAR. The red squares are the 84 x 84 pixels Regions Of Interest (ROI) selected for each forest stand.

400

401 Fluorescence at 690 nm and 740 nm for loblolly pine class ranged between 0.2 and 0.8 mW m^{-2} sr^{-1} nm^{-1}

402 ^{2} sr^{-1} nm^{-1} and between 0.3 and 1.2 mW m^{-2} sr^{-1} nm^{-1}, respectively. Non-fluorescent targets

403 (e.g., the roads between the stands) showed SIF values close to zero, indicating the reliability

404 of the SIF maps. Overall, the SIF emission magnitude of loblolly pine is relatively low

405 compared to dense deciduous forests, as reported in previous studies (Rossini *et al*., 2016) and

406 the values compare well with SIF ground observations obtained over similar loblolly pine

407 stands (ESA, 2015).

408

409 *Reflectance measurements and fAPAR maps*

410 Reflectance and transmittance measurements of loblolly pine needles allowed the computation

411 of the average leaf fAPAR (Figure 4). The proportion of reflected PAR was approximately 8%

412 and the transmitted PAR was ~3%, while the remaining fraction of the total incoming PAR was

413 absorbed (fAPAR = 0.89 or 89%; standard deviation = 0.021). Since at individual leaf level,

414 only about 3% of PAR is transmitted (but subsequently potentially absorbed by other leaves)

415 we are confident that the approach used in this study to generate fAPAR maps may only slightly

416 overestimate canopy fAPAR, and therefore potentially underestimate fluorescence yield.
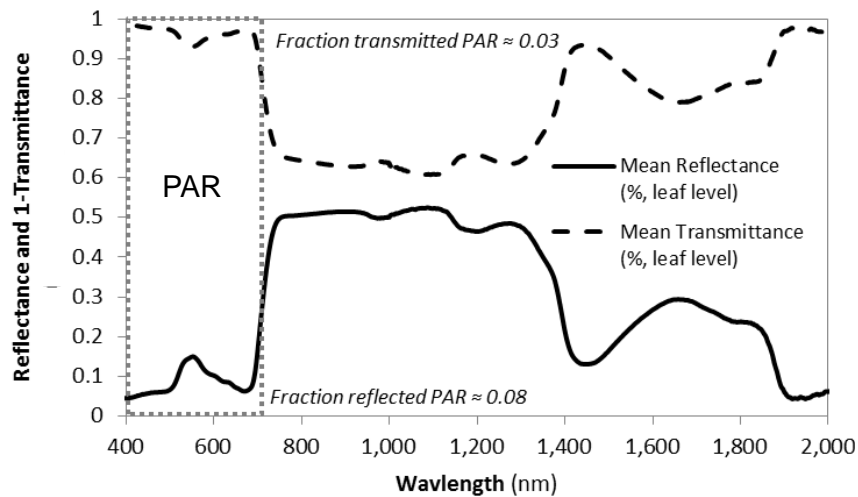
**Fig. 4** Loblolly pine leaf optical properties (mean reflectance and transmittance).

The strong correlation between the two estimates of fAPAR ($R^2= 0.67$ RMSE $= 0.05$, p $<$ 0.001), using the methods previously presented, increases the confidence in our results.

Structural, biophysical, biochemical parameters and leaf gas exchanges

The relationship between tree age and canopy height derived from the G-LiHT LiDAR data at Parker Tract was compared with that measured at the Duke Forest by Drake *et al*., (2010) for pines. A very similar relationship between tree height vs. age was found (Figure 5), suggesting that stands at both forests may belong to the same Site Index and could present similar aging patterns. At the Duke Forest, canopy height ranged from 14 to 43 m, while at the Parker Tract forest tree height varied from 1 to 26 m. Figure 5 shows the relationship between tree age and height for the full dataset including stands from both Parker Tract and Duke Forest modelled using the Gompertz equation (Zeide, 1993).

432
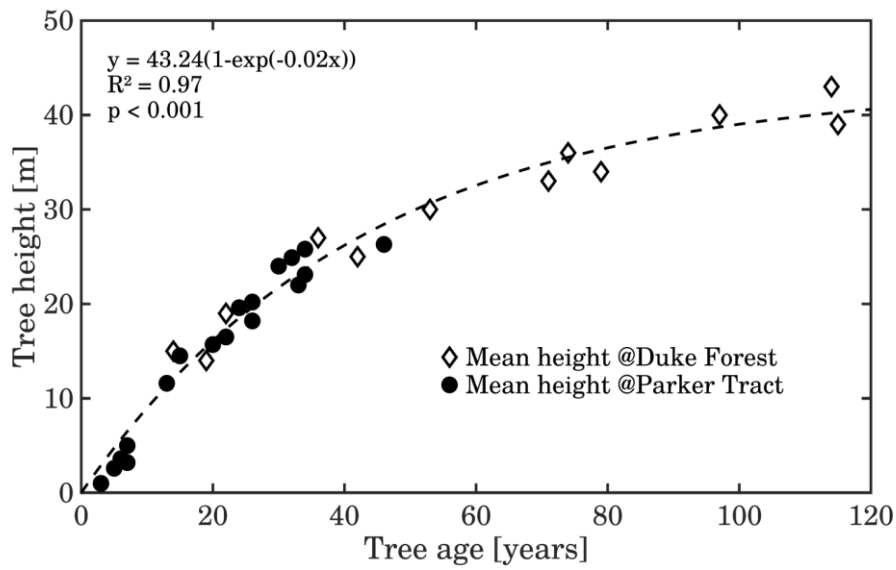
Fig. 5 Relationship between tree height and age at Parker Tract (closed symbols) and Duke

Forest (open symbols, Drake et al., 2010) (R^2=0.97).

Table 1 and Figure 6 show the relationships between stand age and height (in brackets) with

the biophysical and biochemical parameters measured in field and laboratory. These results

clearly show that there were no significant relationships between these variables.

Relationships	R^2	p-value
Age (height) vs. Cab	0.01 (0.01)	0.68 (0.68)
Age (height) vs. LAI	0.13 (0.13)	0.06 (0.04)
Age (height) vs. C	0.05 (0.06)	0.26 (0.22)
Age (height) vs. N	0.03 (0.03)	0.42 (0.39)

439 **Table 1** Coefficient of determination (R^2) and p-value of the linear relationships between stand

440 age (and height) versus vegetation variables: total chlorophyll content (Cab), Leaf Area Index

441 (LAI), carbon (C) and nitrogen concentration (N).

442
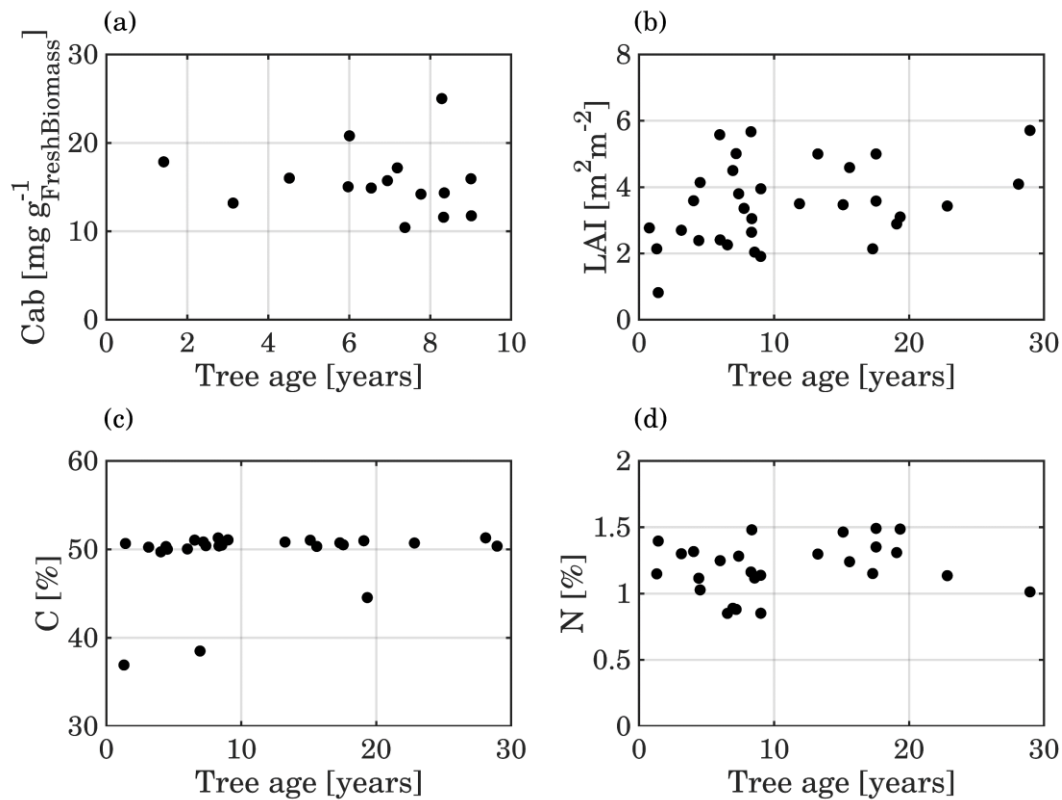
443

444 **Fig. 6**. Scatter plot between loblolly tree age and total Cab (a), LAI (b), C (c) and N (d).

445

446 The leaf level stomatal conductance (g_s; mean and standard error of 6 trees) of young trees was

447 found 82.1 (6.4) / 58.2 (5.8) (mmol $m^{-2} s^{-1}$) in June / September, respectively, while for mature

448 trees it was 61.2 (5.7) / 49.5 (4.2) (mmol $m^{-2} s^{-1}$) in June / September, respectively. P values for

449 both dates between mature and young trees were <0.01. Similarly, leaf level net photosynthesis

450 (P_{net}) of young and mature trees measured in June were 7.0 (0.5) and 5.8 (0.6) μmol $m^{-2} s^{-1}$,

451 respectively, and in September were 5.7 (0.7) and 3.8 (0.6) $\mu mol\ m^{-2}\ s^{-1}$, respectively (p values

452 for both dates for P_{net} between mature and young trees were <0.01). Across stand age, the

453 reduction in P_{net} was highly correlated with the decline in g_s (P_{net} = 0.089 x g_s; R^2 = 0.84; with

454 g_s in mmol $m^{-2}\ s^{-1}$ and P_{net} in $\mu mol\ m^{-2}\ s^{-1}$). Water stress had a larger effect on P_{net} in old trees

455 than in young trees, even though old trees had similar (p=0.42) predawn water potentials in

456 June and even higher (p<0.001) ones (less negative) in September than young trees (data not

457 shown). The decline in P_{net} between June and September was indeed 18.6% in young trees and

458 34.5% in mature trees.

459

460 *Relationship between loblolly fluorescence, APAR, true fluorescence yield and tree age*

461 The relationship between loblolly fluorescence and tree age obtained at Parker Tract is shown

462 in Figure 7. Loblolly SIF was derived by *HyPlant* data at full spatial resolution, while stand age

463 was derived from the Parker Tract management plan (n=18 stands).

24
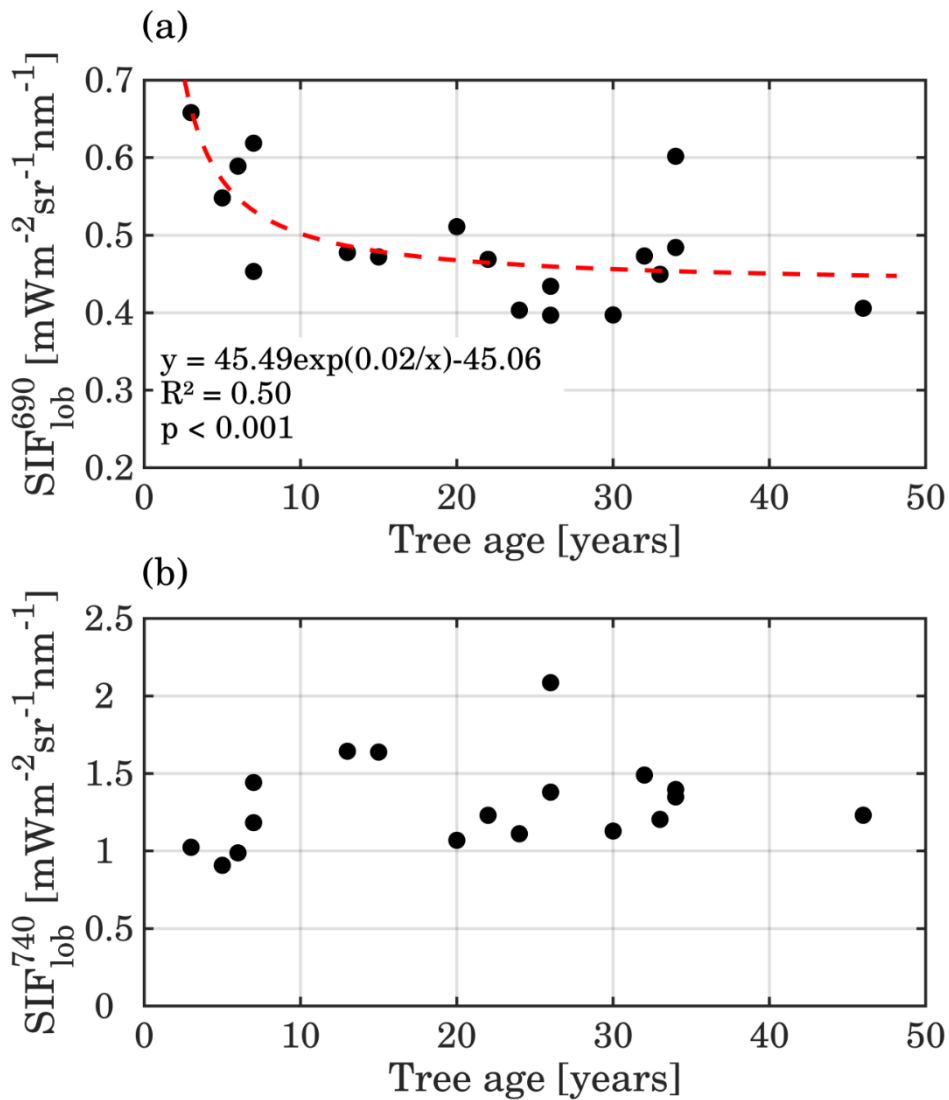
Fig. 7 Mean SIF radiance values (at 690 nm and 740 nm) for the loblolly component, extracted as the average value of the loblolly class in each ROI, and plotted vs. tree age. The far-red SIF radiance is relatively constant so that the SIF vs. tree age relationship is not statistically significant.

Both, SIF_{lob}^{690} and SIF_{lob}^{740} show some variability among stands but only SIF_{lob}^{690} exhibits a statistically significant relationship with tree age. In the case of red fluorescence, a nonlinear decline shows that young forest stands emit slightly more red fluorescence compared to older

473   trees (Fig. 7a). Overall, we tested different models and we found that the exponential model

474   described the data best, producing the highest coefficient of determination.

475   Loblolly APAR shows instead a subtle change with age (Figure 8), with younger stands that

476   absorb less PAR radiation than older canopies.
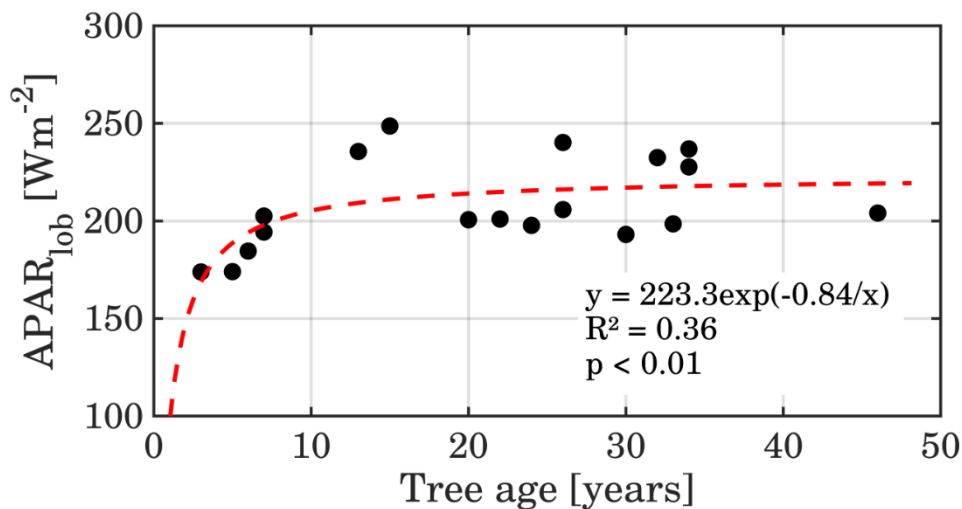
477

478   **Fig. 8** Loblolly APAR values vs. tree age for the 18 ROIs.

479

480   Although there is a link between APAR and SIF, the latter typically shows an additional

481   response to plant physiology and quickly varies with changing photosynthetic activity even

482   before any variation in the pigment pool occurs (e.g., Rossini *et al*., 2015). Hence, the

483   relationship between SIF and APAR is not univocal, and they provide complementary

484   information on different aspects of the photosynthetic process.

485   The relationships between the true red SIF yield and tree age is shown in Figure 9. The nonlinear

486   decrease in ε_{lob}^{690} with age is more pronounced and clearer than for SIF, while there is still no

487   relationship for the far-red SIF yield. True SIF yield performed better than apparent SIF yield

26

488   which was less related to stand age, with results similar to that found for SIF radiance (R^2=0.41,

489   data not shown).
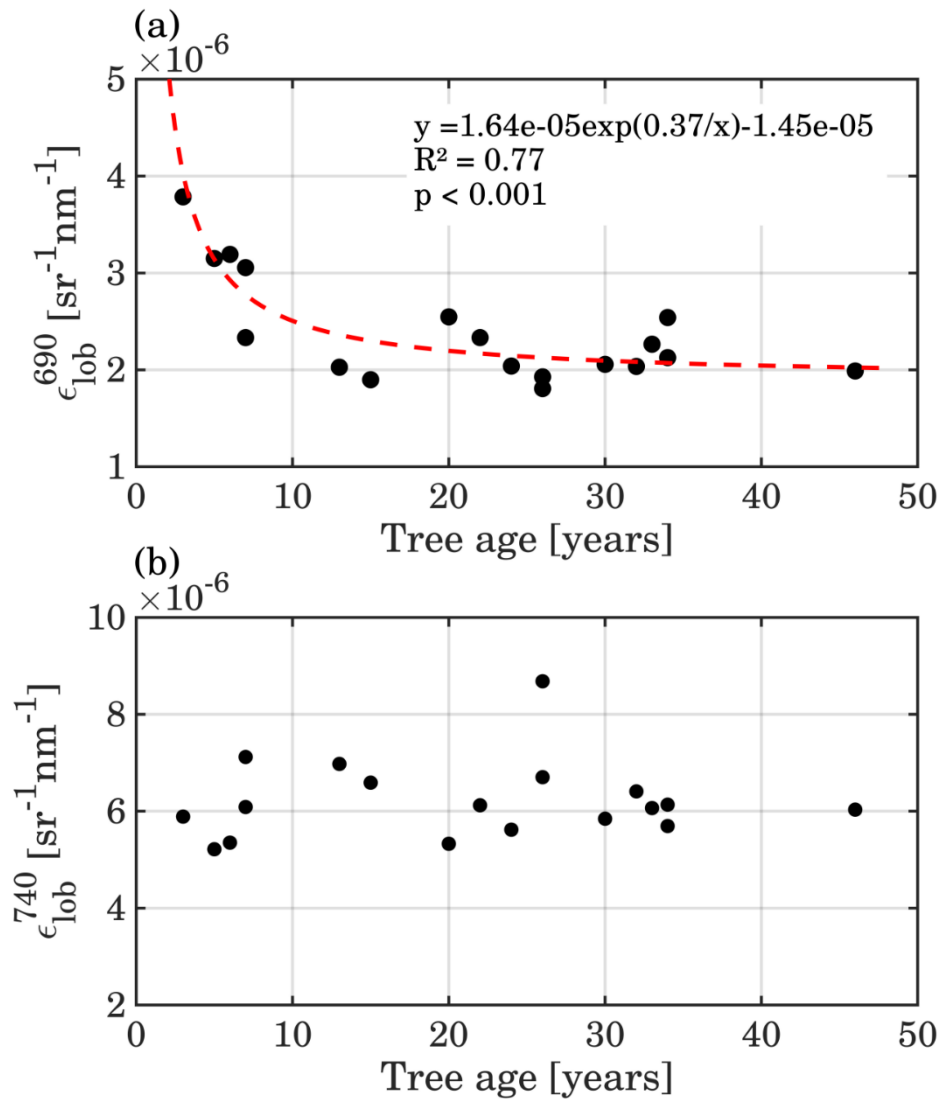
491   **Fig. 9** Red and far-red SIF yields for loblolly pine vs. tree age for observations acquired at 1 m.

493   Overall, young stands exhibiting red SIF yield up to 90% higher than older trees (e.g., 3.8 vs.

494   2.2 sr^{-1} nm^{-1}).

Impact of spatial aggregation on SIF - tree age relationships and performances of the Canopy

497 *Cover Fluorescence Index*

498 The relationships between spatially aggregated (84 m x 84 m) red SIF radiances and true red

499 SIF yield versus stand age are shown in Figure 10. In this case, aggregated pixels are implicitly

500 composed of mixtures of different components.
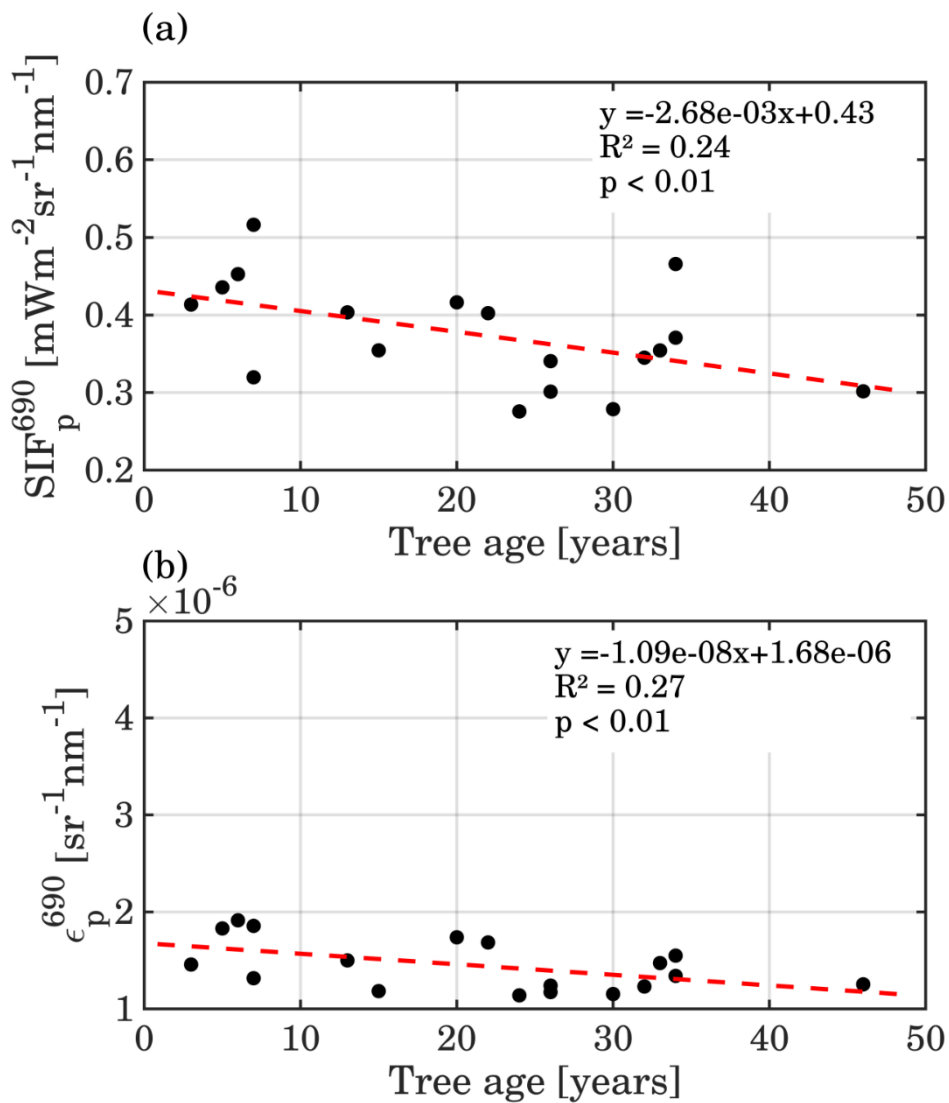
501

502 **Fig. 10** Mean of red SIF radiance (upper panel) and the true red SIF yield (lower panel)

503 computed at coarse spatial resolution (84 m x 84 m) vs. tree age. Note that the axis ranges are

504 deliberatively set equal to those of Figures 7a and 9a, respectively, in order to facilitate visual

505 comparison.

506

507 Although, it is still possible to observe a slight linear decline of both SIF_p^{690} and ε_p^{690} with age,

508 at this coarser spatial resolution this relationship cannot be easily revealed. Similarly,

509 diminishing success for results (in terms of functional relationship and coefficient of

510 determination) were also found when aggregating at 10 m x 10 m, 30 m x 30 m, 60 m x 60 m

511 spatial resolutions (R^2=0.30; R^2=0.27; R^2=0.25, respectively). We underscore that aggregated

512 pixels never resulted in mixed stands with different ages. Such analysis is beyond the scope of

513 this study. In addition, no statistically significant relationships were found between either

514 APAR$_p$ and stand age or $SIF_p{}^{740}$ at different aggregation levels (data not shown).

515 Figure 11a shows the relationship between the fractional cover of the loblolly pine stands and

516 the spatially aggregated red SIF (84 m x 84 m) and indicates that fluorescence is fairly affected

517 by this parameter. The SIF signal at this spatial resolution is in fact a mixture of the fluorescence

518 fluxes emitted by tree crowns, both sunlit and shadowed, and understory with different

519 proportion of bare soils and canopy gaps, which causes a variability in the emitted fluorescence

520 flux over stands with different vegetation cover. Moreover, we also tested the relationship

521 between loblolly fractional cover and tree age we did not find any statistically significant result,

522 although a relevant variability of fractional cover across the different stands (Figure 11b).

523

29
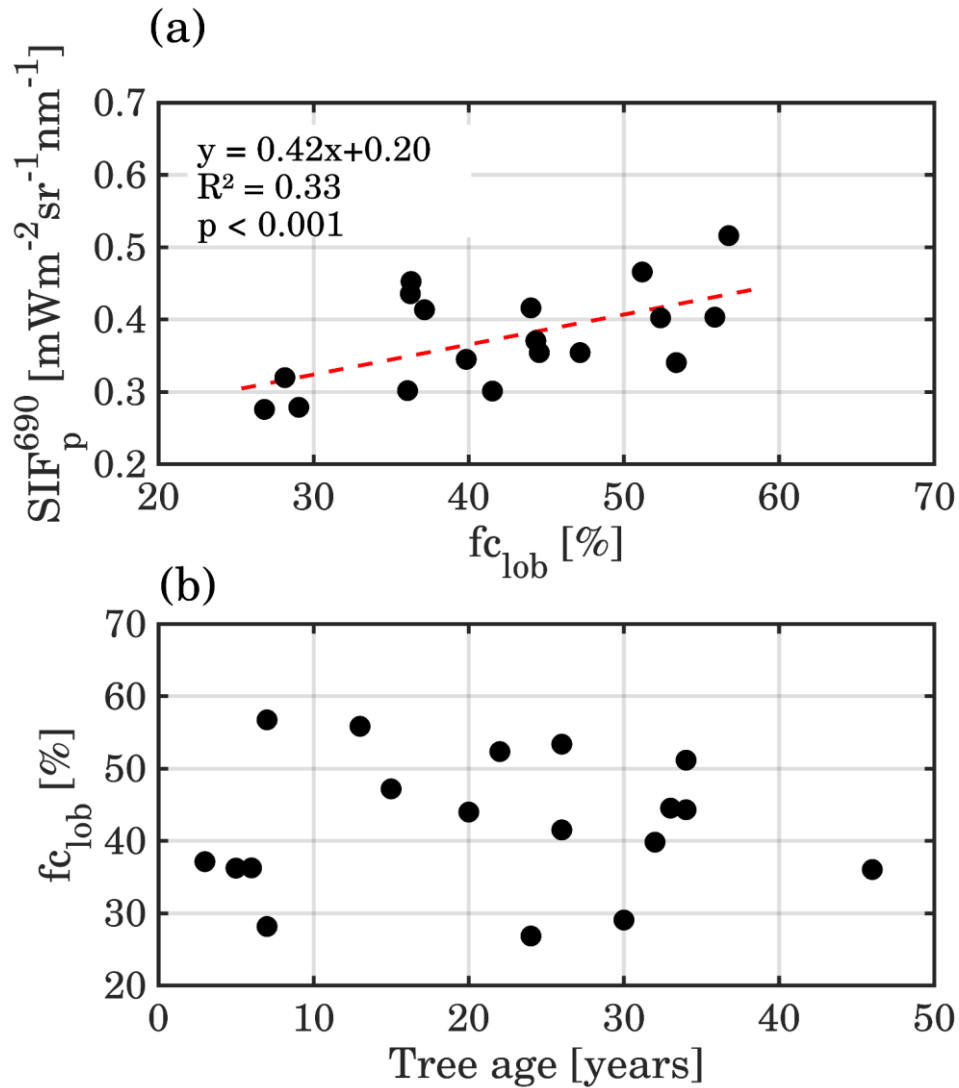
Fig. 11 Relationships between aggregated (84 m x 84 m) red fluorescence and loblolly fractional cover (a), and between fractional cover and tree age (b).

To properly interpret SIF in mixed pixel situations, typical of satellite remote sensing, the spatial variability of vegetation fractional cover has to be taken into account. The relationship between Canopy Cover Fluorescence Index and tree age obtained with aggregated pixel data (84 m x 84 m) is shown in Figure 12.

The figure shows a scatter plot with tree age on the x-axis (0 to 50 years) and $CCFI^{690}$ [$mWm^{-2}sr^{-1}nm^{-1}$] on the y-axis (0.4 to 1.4). A red dashed fit line is shown with the equation:

$$y = 240.6\exp(0.01/x) - 239.8$$
$$R^2 = 0.44$$
$$p < 0.001$$

532
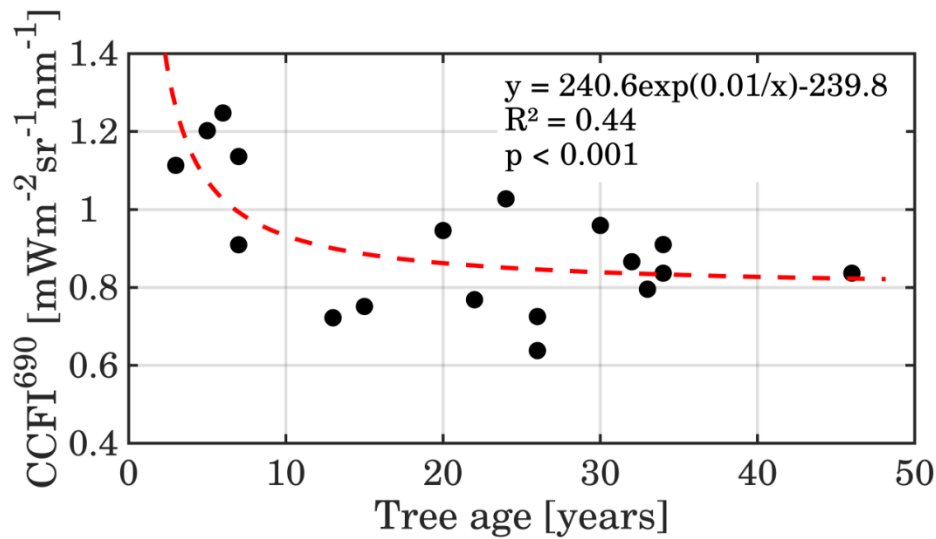
Fig. 12 CCFI computed for aggregated red SIF vs. tree age.

534

Clearly, CCFI is not the same physical quantity as the fluorescence yield, since it is not normalized by APAR. However, it can provide a surrogate of ε_{lob}^{690} with potential to account for sub-pixel heterogeneity in coarse spatial resolution data. The relationship shown in Figure 12, closely resembles those for the loblolly red SIF (Fig. 7a) and its yield (Fig. 9a), providing justification and support for the use of this index in interpreting SIF retrieved from coarse resolution mixed pixels.

541
Discussion

Sun-induced canopy fluorescence and age-related processes

A growing body of evidence demonstrates the relationship between fluorescence yields and photosynthetic rates and it is well known that fluorescence can be used to monitor plant stress at leaf and canopy levels (e.g., Meroni *et al*., 2009; Ac *et al*., 2015). However, the characteristics

547 of sun-induced canopy fluorescence emissions of forest stands of different age have never been

548 investigated. At tree-scale, with *HyPlant* data at full spatial resolution, our results clearly

549 indicate that in loblolly pine: i) red fluorescence and red fluorescence yield change with stand

550 age; measured levels of red SIF were larger in younger trees compared to older ones (up to 60%

551 more SIF_{lob}^{690}) and the decline of ε_{lob}^{690} with stand age (Fig. 9a) is more pronounced than that for

552 red SIF (Fig. 7a), or for the apparent red-fluorescence yield; ii) only SIF_{lob}^{690} and ε_{lob}^{690} declined

553 with tree age, while SIF_{lob}^{740} and ε_{lob}^{740} did not (Figs. 7b, 9b);

554 Overall, the decline of the true red SIF yield with stand age is more informative than for the

555 apparent red SIF yield (the R^2 value for ε_{lob}^{690} is about 87% higher than that for the apparent)

556 and more evident than that found for red SIF radiance itself. The use of the true SIF yield is

557 therefore suitable for suppressing, or mitigating, structural variability and canopy pigment

558 absorption and overall, for comparing spatial measurements collected at different times and

559 under different illumination conditions.

560 No statistically significant relationship was found between LAI, chlorophyll content, carbon

561 and nitrogen concentration with tree height and age (Table 1 and Fig. 6), so that we can

562 reasonably hypothesize that the decline of the red SIF yield with age is not primarily driven by

563 biophysical or biochemical parameters. Consequently, within canopy re-absorption of red SIF

564 radiances should not have a main role in red SIF yield decline related to tree age. The decline

565 of red fluorescence may therefore most likely relate to the underlying physiological processes,

566 that downregulate the photosynthetic activity of the plants during their life cycle. Leaf stomatal

567 conductance measurements and net photosynthesis performed at Parker Tract in September

568 clearly show significant reduction with stand age (7 years old trees=58.2 mmol m^{-2} s^{-1} for g_s and

569 5.7 μmol m^{-2} s^{-1} for P_{net}; 23 years old trees= 49.5 mmol m^{-2} s^{-1} for g_s and 3.8 μmol m^{-2} s^{-1} for P_{net})

570 and potentially explain the drop of red fluorescence with aging. In addition, combining results

571 from predawn water potentials and P_{net} we could determine that mature trees had a reduction in

572 5.5 μmol m^{-2} s^{-1} MPa^{-1}, as opposed to only 2.9 μmol m^{-2} s^{-1} MPa^{-1} for the young trees. Those

573 values indicated that between June and September mature trees were more sensitive to soil

574 drying, and that the decline in soil water content had a larger effect on P_{net} in old trees than in

575 young trees. Since these measurements only refer to two stands of young and mature trees, to

576 better interpret our findings we also exploited the results observed in the loblolly pine forest at

577 Duke Forest, which exhibits similar Site Index (Figure 5) and has been used for relevant

578 investigations in this context (Drake *et al.*, 2010; Noormets *et al.*, 2010; Drake *et al.*, 2011;

579 Domec *et al.*, 2012). Drake *et al.*, (2010 and 2011) showed that light-saturated photosynthetic

580 CO_2 uptake, the concentration of CO_2 within needle air-spaces and stomatal conductance to

581 H_2O declined with tree age due to an increasing water limitation of the plants, while stomatal

582 limitation to net photosynthesis increased, supporting the hydraulic limitation hypothesis as

583 revised by Ryan *et al.*, (2004; 2006). We exploited the stomatal limitation model developed by

584 Drake *et al.*, (2010) and compared it with the observed decline in true red SIF yield, depicting

585 two opposite trends (Figure 13). It is thus plausible to hypothesize that the decline of red SIF

586 yield is a primary consequence of the reduced carbon and water availability induced by the

587 water limitation processes in aging loblolly trees. In other words, the reduced water availability

588 triggers stomata to close, which reduces leaf-internal CO_2 concentrations in the leaf tissue and

589 limits the ability of the carbon fixing enzyme RuBisCO to fix CO_2. This in turn may cause a

590 tailback into the electron transport and finally this is seen in a variation of SIF (Flexas *et al.*,

591 2002; Rascher *et al.,* 2004; Damm *et al* 2010; Ac *et al.*, 2015; Zarco-Tejada *et al.*, 2016). We

592 can also reasonably assume that the decline in red fluorescence is associated with an enhanced

593 non-photochemical quenching in older compared to younger trees, as observed in recent studies

594 (Gamon & Bond, 2013). Moreover, the observed drop in red SIF yield occurs around age 10-

595 15, which for loblolly corresponds to the physiological age of demarcation between juvenile

596 and mature wood (Tasissa & Burkhart 1998). Domec *et al*., 2012 showed that cambial activity

597 is closely related to stomatal conductance, thus further enforcing the link between the observed

598 SIF decline and the increasing water limitation during the physiological maturation process of

599 loblolly pine.
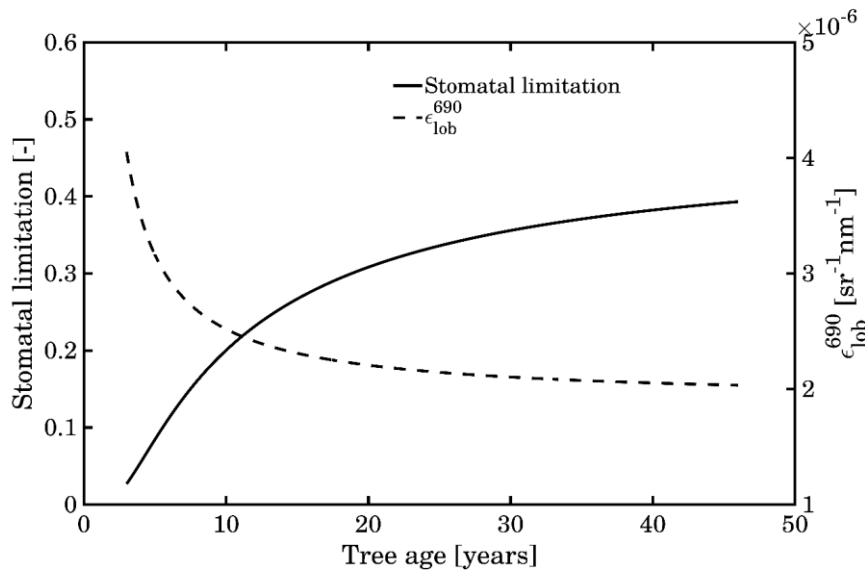
600

601 **Fig. 13** Modelled function of the stomatal limitation in the loblolly chronosequence at Duke

602 Forest using the functional forms derived by Drake et al., (2010) and modelled true red SIF

603 yield of the loblolly pine trees at Parker Tract obtained by the function presented in Figure 9a.

604

605 However, the drop we observed in fluorescence yield is steeper than the increase of stomatal

606 limitation reported at Duke Forest. Our data show in fact a sharp drop in red fluorescence yield

607 before age 10-15 and then a limited change, while at Duke Forest the stomatal limitation clearly

608 increases up to 40 years. Additional studies are therefore needed to fully characterise the link

609 between these trends and to further unravel the role of physiology in driving fluorescence

610 variability. Even though our analysis has been conducted using pure loblolly pixel only, hence

611 minimizing the effect of canopy closure and mutual shading, the description of the radiative

612 transfer in partly or fully shaded pixels, such as the complex stands in Parker Tract, is

613 challenging and therefore we are aware that other functional and structural factors may partially

614 contribute and explain our findings. Changes in leaf structure, needle length, shoot shape

615 (clumping) and wax deposits on leaf surfaces with aging may in fact alter absorption/scattering

616 of red fluorescence, enhancing the observed decrease with age. Therefore, we cannot

617 completely discard a residual influence of canopy structure, a generic scattering effect with

618 aging or changes in specific leaf area before and after canopy closure, which is reached at stand

619 age of approximately 10 years. In addition, the complex canopy structure of the older pine trees

620 not only subtly increases the APAR but may also produce stronger reabsorption of the red

621 fluorescence within the canopy and therefore reduce the measured top-of-canopy fluorescence.

622 In this study we have addressed the change in SIF properties from juvenile to mature stands,

623 however future research, considering the natural lifespan of the loblolly trees of 100+ years of

624 age (Burns & Honkala, 1990), is needed to confirm our findings. Moreover, accurate

625 determination of true SIF yield should require an estimation of PAR absorbed by green leaves

626 (e.g., Gitelson & Gamon, 2015; Zhang *et al*., 2016) and this could be another key point that

627 should be considered for future investigations.

628 Although a statistically significant decreasing trend is clearly recognisable in the true red-SIF

629 yield values as plants become older, no significant relationship with tree age was found with

630 the far-red SIF radiance or yield (Figs. 7b, 9b). The fact that red fluorescence, rather than far-

631 red, seems more sensitive to describe these physiological processes can be considered in line

632 with the recent study of Verrelst *et al*., (2016), which found the red fluorescence as the most

633 sensitive to the canopy net-photosynthesis. Unfortunately, only a few recent studies (Louis et

634 al., 2005; Cheng *et al*., 2013; Rossini *et al.,* 2015; Middleton *et al*., 2015; Wieneke *et al*., 2016;

635 Joiner *et al.*, 2016; Goulas *et al*., 2017) exploiting both red SIF and far-red SIF have been

636 conducted, and future investigations are necessary to consolidate the results found in this study.

637 If fluorescence yield changes as trees age, new information will be needed to account for

638 variations in vegetation age classes across landscapes. However, we do not currently know the

639 behaviour of fluorescence (or its efficiency) when other species- and age-related processes are

640 involved (e.g., within the hypothesis of nutrient limitation) nor do we know how fluorescence

641 behaves across different ecosystems. Consequently, the relationship between fluorescence and

642 tree age reported here cannot be generalized or used to track age classes. Further studies,

643 especially dedicated experiments and modelling activities, may help in understanding how the

644 fluorescence dynamics can contribute to a better description of the environment, age-related

645 dynamics and climate interactions. The use of models incorporating fluorescence (e.g., van der

646 Tol *et al*., 2009; Hernández-Clemente *et al*., 2017) coupled with ecosystem process model for

647 estimating storage and flux of carbon, nitrogen and water (e.g., BIOME-BGC, Running &

648 Gower, 1991) in future research may help in better describing and understanding the role of

649 fluorescence in age-related processes.

650

651 *The need to use normalized SIF metrics at coarse resolution scale*

652 Although new progress has been made in the methodological and technical aspects of

653 fluorescence signal retrieval from space, as shown in recently published global maps (e.g.,

654 Joiner *et al*., 2016), there are definite limitations for SIF interpretation based on large satellite

655 pixels (e.g., GOME-2, 40x80 km; GOSAT, 10x10 km), which are inevitably comprised of

656 mixed components. Although several orbital missions acquire far-red SIF at better spatial

657 resolutions (e.g., OCO-2, 2x2 km; and the upcoming ESA TROPOMI/Sentinel-5P, 7x7 km),

658   the possibility to acquire red SIF is not yet available from space at these resolutions. Some of

659   these disadvantages will be mitigated with the advent of the FLEX mission, which will provide

660   complete fluorescence emission spectra globally, including red SIF, at an ecologically relevant

661   spatial scale of 0.3x0.3 km, thus reducing the mixture problems currently encountered. The

662   intra-pixel mixture effect is a confounding factor for SIF signal interpretation and it should be

663   mitigated wherever possible and only after understanding the impact of spatial scale on the SIF

664   signal, it will be possible to properly exploit the use of fluorescence for plant status or for

665   biomass applications in heterogeneous landscapes.

666   For coarse spatial resolution remote sensing observations, the computation and interpretation

667   of the true fluorescence yield (as presented in Eqs. 4 and 5) is challenging, due to the challenge

668   in characterization of SIF and APAR for pure target vegetation components. Our results indicate

669   that the mixing of components at coarse spatial resolutions can be considered a 'contamination'

670   that hinders the analyses and obscures the relationships between fluorescence and tree age, so

671   that they are no longer clearly detectable in the aggregated (coarse) pixels. Results from analysis

672   with spatially aggregated data at stand-scale revealed that the relationships between red SIF

673   radiances and yields (Fig. 10a, b) were substantially weakened by spatial averaging. In fact, the

674   statistical success in describing the relationship for red SIF yield was reduced by almost 60%

675   (R^2: 0.65 → 0.27, Figs. 9a, 10b) and for red SIF radiances by ~50% (R^2: 0.45 → 0.24, Figs. 7a,

676   10a), and the aggregated trends appeared more linear, solely due to spatial aggregation from 1

677   m to 84 m. To mitigate the impact of surface heterogeneity, we propose the CCFI, which was

678   able to produce acceptable results across a range of spatial resolutions (Fig. 12). In the use of

679   the CCFI, the fc_{lob} normalization may be closely related to the fraction of Intercepted PAR

680   (Pickett-Heaps *et al*., 2014), while less related to the amount of canopy pigments and stand

681   darkness. Thus, CCFI, by exploiting fractional cover, seems able to minimize the effects of

682 canopy structure, enhancing differences in the fluorescence yield of young and old loblolly pine

683 trees.

684 The vegetation fractional cover is a key vegetation parameter that has already been successfully

685 produced using different remote sensing techniques, by exploiting optical or LiDAR imagery,

686 from several current and past airborne or satellite data operating at different spatial and temporal

687 resolutions (e.g., Chen & Cihlar, 1996; Carlson & Ripley; 1997; Gutman & Ignatov, 1998;

688 North, 2002; Latifovic & Olthof, 2004; Jimenez *et al*., 2005; Baret *et al*., 2007; Olthof & Fraser,

689 2007; Verhoef & Bach, 2007; Busetto *et al*., 2008). In the context of the FLEX mission,

690 vegetation fractional cover could be dynamically derived at higher spatial resolution from

691 Landsat or Sentinel-2 like missions and then incorporated into the FLEX processing chain to

692 compute the CCFI. The vegetation fractional cover can be more easily estimated than APAR

693 from classification techniques and land use/cover maps. The real benefit in using fractional

694 cover rather than APAR as a normalization tool is that it is more independent of illumination

695 conditions and more stable in time. Thus, it is not mandatory to measure or compute it

696 simultaneously with fluorescence, although it is necessary for APAR, an instantaneous quantity

697 highly dependent on time of acquisition, as fluorescence is. For the satellite perspective, the

698 cosine of the zenith angle normalization can be added to CCFI to take into account the effects

699 of temporal variability of incoming PAR.

700 The computation of CCFI is quite straightforward since it only requires, in addition to SIF

701 radiances, the knowledge of the fractional vegetation cover in each pixel. However, this

702 normalization cannot be considered as a replacement of the true SIF yield, but rather a

703 complementary index that can be used under specific assumptions. CCFI is not applicable in a

704 general framework at canopy level with airborne or satellite measurements, but only in some

705 conditions, where two components with high fluorescence contrast contribute to the recorded

signal. For savannah-like ecosystems, forests without understory and crops in certain phenological phases, this normalization technique may help to better detect plant status and processes. This index is not particularly suited for fragmented agricultural landscapes with different crops within the same pixel or for complex mixed forests, and therefore additional studies are needed to define strategies for global scale applications. Moreover, further studies exploiting new emerging 3-D radiative transfer models incorporating fluorescence, like FluorWPS (Zhao *et al.*, 2016), FluorFLIGHT (Hernández-Clemente *et al.*, 2017) and DART (Gastellu-Etchegorry *et al.*, 2017) will help to test the performance of CCFI and the effects caused by the canopy structure on the fluorescence signal recorded from mixed pixels. In summary, the CCFI index can be applied, under certain conditions, to coarse spatial resolution data to minimize confounding factors due to the spatial variability of canopy structure, and it is expected to be suitable for applications assessing vegetation function in future Earth Observations in the fluorescence era.

730

731 **References**

732 Ac A, Malenovsky Z, Olejnickova J, Gallé A, Rascher U, and Mohammed G, (2015) Meta-
733 analysis assessing potential of steady-state chlorophyll fluorescence for remote sensing
734 detection of plant water, temperature and nitrogen stress. *Remote Sensing of Environment*, 168,
735 420–436.

736 Baret F, Hagolle O, Geiger B, Bichero P, Miras B, Huc M, Berthelot B, Nino F, Weiss M,
737 Samain O, Roujean JL and Leroy M, (2007) LAI, fAPAR and fCover CYCLOPES global
738 products derived from VEGETATION. Part 1: Principles of the algorithm. *Remote Sensing of*
739 *Environment*, 110(3), 275–286.

740 Bond, B, (2000) Age-related changes in photosynthesis of woody plants. *Trends in Plant*
741 *Science,* (5)8, 349-353.

742 Burns RM, & Honkala BH, (1990) Silvics of North America, Vol. 1, Conifers. Washington DC:
743 *U.S.D.A. Forest Service Agriculture Handbook* 654.

744 Busetto L, Meroni M, Colombo R, (2008) Combining medium and coarse spatial resolution
745 satellite data to improve the estimation of sub-pixel NDVI time series. *Remote Sensing of*
746 *Environment*, 112(1), 118-131.

747 Carlson TN, & Ripley DA, (1997) On the relation between NDVI, fractional vegetation cover,
748 and leaf area index. *Remote Sensing of Environment*, 62(3), 241–252.

749 Cerovic ZG, Goulas Y, Gorbunov M, Briantais JM, Camenen L, Moya I, (1996) Fluorosensing
750 of water stress in plants: Diurnal changes of the mean lifetime and yield of chlorophyll
751 fluorescence, measured simultaneously and at distance with a τ-LIDAR and a modified PAM-

752 fluorimeter, in maize, sugar beet, and kalanchoë, *Remote Sensing of Environment*, 58(3), 311–

753 321.

754 Chapelle EW, & Kim MS. (1992) Ratio analysis of reflectance spectra (RARS): an algorithm

755 for the remote estimation of the concentration of chlorophyll a, Chlorophyll b, and carotenoids

756 in soybean leaves. *Remote Sensing of Environment*, 39, 239-247.

757 Chen JM. & Cihlar J, (1996) Retrieving leaf area index for boreal conifer forests using Landsat

758 TM images. *Remote Sensing of Environment,* 55,153-162.

759 Cheng YB, Middleton E, Zhang, *et al*., (2013) Integrating Solar Induced Fluorescence and the

760 Photochemical Reflectance Index for Estimating Gross Primary Production in a Cornfield.

761 *Remote Sensing,* 5, 6857-6879.

762 Cogliati S, Verhoef W, Kraft S, Sabater N, Alonso L, Vicent J, Moreno, J, Drusch M. and

763 Colombo R, (2015) Retrieval of sun-induced fluorescence using advanced spectral fitting

764 methods. *Remote Sensing of Environment*, 169, 344–357.

765 Colombo R, Meroni M, Rossini M, (2016) Development of fluorescence indices to minimize

766 the effects of canopy structural parameters, *Annali di Botanica*, 6, 93–99.

767 Cook BD, Corp LA, Nelson RF, Middleton EM. Morton DC, McCorkel JT, Masek JG, Ranson,

768 KJ, Ly V, Montesano PM, (2013) NASA Goddard's Lidar, Hyperspectral and Thermal (G-

769 LiHT) airborne imager. *Remote Sensing*. 5,4045-4066.

770 Damm A, Elbers J, Erler A, Gioli B, Hamdi K, Hutjes R, Kosvancova M, Meroni, M, Miglietta

771 F, Moersch A, Moreno J, Schickling A, Sonnenschein R, Udelhoven T, Van Der Linden S,

772 Hostert P and Rascher U, (2010) Remote sensing of sun-induced fluorescence to improve

773   modeling of diurnal courses of gross primary production (GPP). *Global Change Biology*, 16(1),

774   171–186.

775   Damm A, Guanter L, Verhoef W, Schläpfer D, Garbari S. and Schaepman ME, (2015a). Impact

776   of varying irradiance on vegetation indices and chlorophyll fluorescence derived from

777   spectroscopy data. *Remote Sensing of Environment*, 156, 202-215.

778   Damm A, Guanter L, Paul-Limoges E, van der Tol C, Hueni A, Buchmann N, Eugster W,

779   Ammann C, and Schaepman ME, (2015b) Far-red sun-induced chlorophyll fluorescence shows

780   ecosystem-specific relationships to gross primary production: An assessment based on

781   observational and modeling approaches. *Remote Sensing of Environment*, 166, 91–105.

782   Daumard F, Champagne S, Fournier A, Goulas Y, Ounis A, Hanocq JF, Moya I, (2010) A field

783   platform for continuous measurement of canopy fluorescence. *IEEE Transactions on*

784   *Geoscience and Remote Sensing*, 48(9), 3358–3368.

785   de Beeck MO, Gielen B, Jonckheere I, Samson R, Janssens IA, Ceulemans R, (2010) Needle

786   age-related and seasonal photosynthetic capacity variation is negligible for modelling yearly

787   gas exchange of a sparse temperate Scots pine forest. *Biogeosciences*, 7(1), 199–215.

788   D'Odorico P, Gonsamo A, Pinty B, Gobro, N, Coops N, Mendez E, Schaepman ME, (2014)

789   Intercomparison of fraction of absorbed photosynthetically active radiation products derived

790   from satellite data over Europe. *Remote Sensing of Environment*, 142, 141-154.

791   Domec JC & Gartner BL, (2003) Relationship between growth rates and xylem hydraulic

792   characteristics in young, mature and old-growth ponderosa pine trees. *Plant, Cell and*

793   *Environment*, 26, 471–83.

794 Domec JC, Sun G, Noormets A, Gavazzi MJ, Treasure EA, Cohen E, Swenson JJ, McNulty S

795 G and King JS, (2012) A comparison of three methods to estimate evapotranspiration in two

796 contrasting loblolly pine plantations: Age-related changes in water use and drought sensitivity

797 of evapotranspiration components. *Forest Science*, 58(5), 497–512.

798 Domec JC, King JS, Ward E, Oishi AC, Palmroth S, Radecki A, Bell DM, Miao G, Gavazzi

799 M, Johnson DM, McNulty SG, Sun G, Noormets A, (2015) Conversion of natural forests to

800 managed forest plantations decreases tree resistance to prolonged droughts. *Forest Ecology and*

801 *Management,* 355, 58-71.

802 Domec JC, Lachenbruch B, Pruyn M, and Spicer R, (2012) Effects of age-related increases in

803 sapwood area, leaf area, and xylem conductivity on height-related hydraulic costs in two

804 contrasting coniferous species. *Annals of Forest Science,* 69, 17-27.

805 Donohue RJ, Roderick ML, & McVicar TR, (2008) Deriving consistent long-term vegetation

806 information from AVHRR reflectance data using a cover-triangle-based framework. *Remote*

807 *Sensing of Environment*, 112, 2938-2949.

808 Drake JE, Raetz LM, Davis SC, & Delucia EH, (2010) Hydraulic limitation not declining

809 nitrogen availability causes the age-related photosynthetic decline in loblolly pine (Pinus taeda

810 L.): Loblolly pine photosynthesis. *Plant, Cell & Environment*, 33(10), 1756–1766.

811 Drake JE, Davis SC, Raetz LM, & Delucia EH, (2011) Mechanisms of age-related changes in

812 forest production: The influence of physiological and successional changes. *Global Change*

813 *Biology*, 17(4), 1522–1535.

814 Drusch M, Moreno J, Del Bello U, Franco R, Goulas Y, Huth A, Kraft S, Middleton E, Miglietta

815 F, Mohammed G, Nedbal L, Rascher U, and Schuttemeyer D, (2017) The FLuorescence

816 EXplorer (FLEX) mission concept – ESA's Earth Explorer 8. *IEEE TGRS*, 55, 3, 1273.

817   ESA, (2015) FLEX-US Final Report, Technical Assistance for the Deployment of the Airborne

818   HyPlant Imaging Spectrometer during 2013 ESA/NASA Joint FLEX-US (FLuorescence

819   EXplorer Experiment in USA) Campaign.

820   ESA, (2017) FLEX-EU Final Report, Technical Assistance for the Deployment of an advanced

821   hyperspectral-imaging sensor during FLEX-EU Campaign.

822   Flexas J, Escalona JM, Evain S, Gulías J, Moya I, Osmond CB, Medrano H, (2002) Steady state

823   chlorophyll fluorescence (Fs) measurements as a tool to follow variations of net CO2

824   assimilation and stomatal conductance during water-stress in C3 plants, *Physiol. Plant.*,114(2),

825   231– 240.

826   Fournier A, Daumard F, Champagne S, Ounis A, Goulas Y, Moya I, (2012) Effect of canopy

827   structure on sun-induced chlorophyll fluorescence. *ISPRS Journal of Photogrammetry and*

828   *Remote Sensing*, 68(1), 112–120.

829   Gamon JA & Bond B, (2013) Effects of irradiance and photosynthetic downregulation on the

830   photochemical reflectance index in Douglas-fir and ponderosa pine. *Remote sensing of*

831   *Environment,* 135, 141-149.

832   Gastellu-Etchegorry JP, Lauret N, Yin T, Landier L, Kallel A, Malenovsky Z, Al Bitar A, Aval

833   J, Benhmida S, Qi J, Medjdoub J, Guilleux J, Chavanon E, Cook B, Morton D, Chrysoulakis

834   N, and Mitraka Z, (2017). DART: Recent advances in remote sensing data modelling with

835   atmosphere, polarization, and chlorophyll fluorescence, *IEEE J. Sel. Topics Appl. Earth*

836   *Observ. Remote Sens.*, 10(6), 2640–2649.

837   Gitelson AA, & Gamon JA, (2015) The need for a common basis for defining light-use

838   efficiency: Implications for productivity estimation. *Remote Sensing of Environment,* 156, 196-

839   201.

840 Gobron N, Pinty B, Taberner M, Melin F, Verstraete MM, Widlowski JL, (2006) Monitoring

841 the photosynthetic activity of vegetation from remote sensing data. *Advances in Space*

842 *Research*, 38, 2196-2202.

843 Goulas Y, Fournier A, Daumard F, Champagne S, Ounis A, Marloie O, Moya I, (2017) Gross

844 Primary Production of a Wheat Canopy Relates Stronger to Far Red Than to Red Solar-Induced

845 Chlorophyll Fluorescence. *Remote Sensing*, 9(1), 97.

846 Goward SN, & Huemmrich KF, (1992) Vegetation canopy PAR absorptance and the

847 normalized difference vegetation index: An assessment using the SAIL model, *Remote sensing*

848 *of Environment* 39,119-140.

849 Gower ST McMurtrie RE, Murty D, (1996) Aboveground net primary production decline with

850 stand age: potential causes. *Trends Ecol. Evol.*, 11, 378–382.

851 Greenwood M.S, (1995) Juvenility and maturation in conifers: current concepts. *Tree Physiol*.

852 15, 433–438.

853 Guanter L, Frankenberg C., Dudhia A, Lewis PE, Gomez-Dans J, Kuze A, and Grainger RG,

854 (2012) Retrieval and global assessment of terrestrial chlorophyll fluorescence from GOSAT

855 space measurements. *Remote Sensing of Environment*, 121, 236–251.

856 Guanter L, Rossini M, Colombo R, Meroni M, Frankenberg C, Lee JE, and Joiner J, (2013)

857 Using field spectroscopy to assess the potential of statistical approaches for the retrieval of sun-

858 induced chlorophyll fluorescence from ground and space. *Remote Sensing of Environment*, 133,

859 52–61.

860 Guanter L, Zhang Y, Jung M, Joiner J, Voigt M, Berry JA, Frankenberg C, Huete AR, Zarco-

861 Tejada PJ, Lee J, Moran SM, Ponce-Campos G, Beer C, Camps-Valls G, Buchmann N,

862   Gianelle, D, Klumpp K, Cescatti A, Baker JM and Griffis TJ, (2014) Global and time-resolved

863   monitoring of crop photosynthesis with chlorophyll fluorescence. *Proceedings of the National*

864   *Academy of Sciences*, 201320008.

865   Gutman G, & Ignatov A, (1998) The derivation of the green vegetation fraction from

866   NOAA/AVHRR for use in numerical weather prediction models. *Int. J. Remote Sensing*, 19,

867   1533-1543.

868   Hatfield JL, Asrar G, and Kanemasu ET, (1984) Intercepted photosynthetically active radiation

869   estimated by spectral reflectance, *Remote sensing of Environment,* 14, 65-75.

870   Hernández-Clemente R, North PRJ, Hornero A, and Zarco-Tejada PJ, (2017) Assessing the

871   effects of forest health on sun-induced chlorophyll fluorescence using the FluorFLIGHT 3-D

872   radiative transfer model to account for forest structure. *Remote Sensing of Environment*, 193,

873   165–179.

874   Hoge FE, Swift RN, and Yungel JK, (1983) Feasibility of airborne detection of laser-induced

875   fluorescence emissions from green terrestrial plants. *Appl. Opt*. 22(19), 2991-3000.

876   Hubbard RM, Yoder BJ, and Ryan MG, (1999) Evidence that hydraulic conductance limits

877   photosynthesis in old Pinus ponderosa trees. *Tree Physiology*, 19, 165–172.

878   Jiménez-Muñoz JC, Sobrino JA, Guanter L, Moreno J, Plaza A. and Martínez P, (2005)

879   Fractional Vegetation Cover Estimation from PROBA/CHRIS Data: Methods, Analysis of

880   Angular Effects and Application to the Land Surface Emissivity. *3rd ESA CHRIS/Proba*

881   *Workshop* 21-23 March, ESRIN (Frascati, Italy).

882   Joiner J, Yoshida Y, Vasilkov AP, Schaefer K, Jung M, Guanter L, Zhang Y, Garrity S,

883   Middleton EM, Huemmrich KF, Gu L, and Belelli Marchesini L, (2014) The seasonal cycle of

884 satellite chlorophyll fluorescence observations and its relationship to vegetation phenology and

885 ecosystem atmosphere carbon exchange. *Remote Sensing of Environment*, 152, 375–391.

886 Joiner J, Yoshida Y, Guanter L, Middleton EM, (2016) New methods for retrieval of

887 chlorophyll red fluorescence from hyper-spectral satellite instruments: simulations and

888 application to GOME-2 and SCIAMACHY. *Atmos Meas Tech Discuss.*, 1–41.

889 Knyazikhin Y, Schull MA, Stenberg P, Mottus M, Rautiainen M, Yang Y, Marshack A, Latorre

890 Carmona P, Kaufmann KR, Lewis P, Disney MI, Vanderbilt V, Davis AB, Baret F, Jacquemoud

891 S, Lyapustin A. and Myneni RB, (2012) Hyperspectral remote sensing of foliar nitrogen

892 content. *Proceedings of the National Academy of Sciences*, 110(3), E185–E192.

893 Koffi EN, Rayner PJ, Norton AJ, Frankenberg C, and Scholze M, (2015) Investigating the

894 usefulness of satellite-derived fluorescence data in inferring gross primary productivity within

895 the carbon cycle data assimilation system. *Biogeosciences*, 12(13), 4067–4084.

896 Larcher W, (1969) The effect of environmental and physiological variables in the carbon

897 dioxide exchange of trees. *Photosynthetica*, 3, 16.

898 Latifovic R, & Olthof J, (2004) Accuracy assessment using sub-pixel fraction error matrices of

899 global land cover products derived from satellite data. *Remote Sensing of Environment*, 90,

900 153–165.

901 Lee JE, Frankenberg C, van der Tol C, Berry JA, Guanter L, Boyce CK, Fisher J B, Morrow E,

902 Worden JR., Asefi S, Badgley G, and Saatchi S, (2013) Forest productivity and water stress in

903 Amazonia: Observations from GOSAT chlorophyll fluorescence. *Proc Biol Sci.,* 280(1761),

904 20130171.

905 Linkosalo T, Heikkinen J, Pulkkinen P, and Mäkipää R, (2014) Fluorescence measurements

906 show stronger cold inhibition of photosynthetic light reactions in Scots pine compared to

907 Norway spruce as well as during spring compared to autumn. *Frontiers in Plant Science.*

908 Liu L, Guan L, and Liu X, (2017) Directly estimating diurnal changes in GPP for C3 and C4

909 crops using far-red sun-induced chlorophyll fluorescence. *Agricultural and Forest*

910 *Meteorology*, 232, 1–9.

911 Louis JA, Ounis JM, Ducruet S, Evain T, Laurila T, Thum M, Aurela M, Wingsle G, Alonso

912 L, Pedros R, Moya I, (2005) Remote Sensing of Sunlight-Induced Chlorophyll Fluorescence

913 and Reflectance of Scots Pine in the Boreal Forest during Spring Recovery. *Remote Sensing of*

914 *Environment* 96 (1), 37–48.

915 Malenovský Z, Homolová L, Zurita-Milla R, Lukeš P, Kaplan V, Hanuš J, Gastellu-Etchegorry

916 JP, and Schaepman ME, (2013) Retrieval of spruce leaf chlorophyll content from airborne

917 image data using continuum removal and radiative transfer. *Remote Sensing of Environment*,

918 131, 85–102.

919 Maier CA, Palmroth S, and Ward E, (2008) Branch growth and gas exchange in 13-year-old

920 loblolly pine (Pinus taeda) trees in response to elevated carbon dioxide concentration and

921 fertilization. *Tree Physiology* 28, 1093–1106.

922 Meinzer FC, Lachenbruch B, and Dawson TE, (2011) Size- and Age-Related Changes in Tree

923 Structure and Function. *Springer Science & Business Media, 514 pages*.

924 Meroni M, & Colombo R, (2006) Leaf level detection of solar induced chlorophyll fluorescence

925 by means of a subnanometer resolution spectroradiometer. *Remote Sensing of Environment*,

926 103(4), 438–448.

927 Meroni M, Rossini M, Picchi V, Panigada C, Cogliati S, Nali C, and Colombo R, (2008)

928 Assessing Steady-state Fluorescence and PRI from Hyperspectral Proximal Sensing as Early

929 Indicators of Plant Stress: The Case of Ozone Exposure. *Sensors*, 8(3), 1740–1754.

930 Meroni M, Rossini M, Guanter L, Alonso L, Rascher U, Colombo R, and Moreno J, (2009)

931 Remote sensing of solar-induced chlorophyll fluorescence: Review of methods and

932 applications. *Remote Sensing of Environment*, 113(10), 2037–2051.

933 Middleton EM, Huemmrich KF, Cheng YB, and Margolis HA, (2012) Spectral bio-indicators

934 of photosynthetic efficiency and vegetation stress, In Hyperspectral Remote Sensing of

935 Vegetation, Editors: P.S. Thenkabail, J.G. Lyon, and A. Huete, Taylor & Francis, (Cat. #

936 K12019).

937 Middleton EM, Cheng YB, Campbell PE, Huemmrich KF, Corp LA, Bernardes S, Zhang Q,

938 Landis DR, Kustas WP, Daughtry CST, and Russ AL, (2015) Multi-angle hyperspectral

939 observations with SIF and PRI to detect plant stress & GPP in a cornfield. *Proceedings, 9th*

940 *EARSeL SIG Workshop on Imaging Spectroscopy*, CD-ROM, Luxembourg City, Luxembourg,

941 April 2015, 10 pp.

942 Middleton EM, Rascher U, Corp LA, Huemmrich FK, Cook BD, Noormets A, Schickling A,

943 Pinto F, Alonso L, Damm A, Guanter L, Colombo R, Campbell PKE, Landis DR, Zhang Q,

944 Rossini M, Schuettemeyer D, Bianchi R, (2017) The 2013 FLEX-US Airborne Campaign at

945 the Parker Tract Loblolly Pine Plantation in North Carolina, USA. *Remote Sensing*, 9(6), 612.

946 Moya I, Camenenb L, Evain S, Goulas Y, Cerovic ZG, Latouche G, Flexas J, and Ounis A,

947 (2004) A new instrument for passive remote sensing: 1. Measurements of sunlight-induced

948 chlorophyll fluorescence. *Remote Sensing of Environment,* 91, 186−197.

949   Moya I, Daumard F, Moise N, Ounis A, and Goulas Y, (2006) First airborne multiwavelength

950   passive chlorophyll fluorescence measurements over La Mancha (Spain) fields, *2nd*

951   *International Symposium on Recent Advances in Quantitative Remote Sensing*: RAQRS'II, 25–

952   29th September, Torrent (Valencia)-Spain.

953   Myneni RB, Williams DL, (1994) On the relationship between FAPAR and NDVI. *Remote*

954   *Sensing of Environment*, 49(3), 200–211.

955   Myneni RB, Hoffman S, Knyazikhin Y, Privette JL, Glassy J, Tian Y, Wang Y, Song X, Zhang

956   Y, Smith G.R, Lotsch A, Friedl M, Morisette JT, Votava P, Nemani RR, and Running SW,

957   (2002) Global products of vegetation leaf area and fraction absorbed PAR from year one of

958   MODIS data. *Remote Sensing of Environment*, 83, 214-231

959   Noormets A, Gavazzi M, McNulty SG, Domec JC, Sun G, King JS, and Chen, J, (2010)

960   Response of carbon fluxes to drought in a coastal plain loblolly pine forest. *Global Change*

961   *Biology*, 16, 272–287.

962   North PRJ, (2002) Estimation of fAPAR, LAI, and vegetation fractional cover from ATSR-2

963   imagery. *Remote Sensing of Environment*, 80(1), 114–121.

964   Novick K, Oren R, Stoy P, Juang JY, Siqueira M, and Katul G, (2009) The relationship between

965   reference canopy conductance and simplified hydraulic architecture, *Advances in Water*

966   *Resources,* 32, 09-819.

967   Olioso A, Méthy M, and Lacaze B, (1992) Simulation of canopy fluorescence as a function of

968   canopy structure and leaf fluorescence. Remote Sensing of Environment, 41, 239–247.

969   Olthof, I. and Fraser, R.H., (2007) Mapping northern land cover fractions using Landsat ETM+.

970   *Remote Sensing of Environment*, 107, pp. 496–509.

971   Oren R, Hsieh CI, Stoy P, Albertson J, McCarthy HR, Harrell P, KatulGG, (2006) Estimating

972   the uncertainty in annual net ecosystem carbon exchange: spatial variation in turbulent fluxes

973   and sampling errors in eddy-covariance measurements. *Global Change Biology*, 12, 883–896.

974   Pickett-Heaps CA, Canadell JG, Briggs PR, Gobron N, Haverd V, Paget MJ, Pinty B, Raupach,

975   MR, (2014) Evaluation of six satellite-derived Fraction of Absorbed Photosynthetic Active

976   Radiation (FAPAR) products across the Australian continent. *Remote Sensing of Environment*,

977   140, 241–256.

978   Porcar-Castell A, Tyystjarvi E, Atherton J, van der Tol C, Flexas J, Pfuendel EE, Moreno J,

979   Frankenberg C, and Berry JA, (2014) Linking chlorophyll a fluorescence to photosynthesis for

980   remote sensing applications: mechanisms and challenges. *Journal of Experimental Botany* 65,

981   15, 4065-4095.

982   Quantum GIS Development Team, (2016) Quantum GIS Geographic Information System.

983   Open Source Geospatial Foundation Project, http://qgis.osgeo.org.

984   Rascher U, Bobich EG, Lin GH, Walter A, Morris T, Naumann M, Nichol CJ, Pierce D, Bil K,

985   Kudeyarov V, Berry JA, (2004) Functional diversity of photosynthesis during drought in a

986   model tropical rainforest—the contributions of leaf area, photosynthetic electron transport and

987   stomatal conductance to reduction in net ecosystem carbon exchange. *Plant Cell Environ*. 27,

988   1239-1256.

989   Rascher U, Agati G, Alonso L, Cecchi G, Champagne S, Colombo R, Damm A, Daumard F,

990   de Miguel E, Fernandez G, Franch B, Franke J, Gerbig C, Gioli B, Gómez JA, Goulas Y,

991   Guanter L, Gutiérrez-de-la-Cámara Ó, Hamdi K, Hostert P, Jiménez M, Kosvancova M,

992   Lognoli D, Meroni M, Miglietta F, Moersch A, Moreno J, Moya I, Neininger B, Okujeni A,

993   Ounis A, Palombi L, Raimondi V, Schickling A, Sobrino JA, Stellmes M, Toci G, Toscano P,

994   Udelhoven T, van der Linden S, Zaldei A, (2009) CEFLES2: The remote sensing component

995   to quantify photosynthetic efficiency from the leaf to the region by measuring sun-induced

996   fluorescence in the oxygen absorption bands. *Biogeosciences* 6: 1181-1198

997   Rascher U, Alonso L, Burkart A, Cilia C, Cogliati S, Colombo R, Damm A, Drusch M, Guanter

998   L, Hanus J, Hyvärinen T, Julitta T, Jussila J, Kataja K, Kokkalis P, Kraft S, Kraska T, Matveeva,

999   M, Moreno J, Muller O, Panigada C, Pikl M, Pinto F, Prey L, Pude R, Rossini M, Schickling

1000 A, SchurrU, Schüttemeyer D, Verrelst J, and Zemek F, (2015) Sun-induced fluorescence - a

1001 new probe of photosynthesis: First maps from the imaging spectrometer HyPlant. *Global*

1002 *Change Biology*, 21(12), 4673–4684.

1003 Reinhardt K, Johnson DMJM, and Smith WKSK, (2009) Age-class differences in shoot

1004 photosynthesis and water relations of Fraser fir (Abies fraseri), southern Appalachian

1005 Mountains, USA. *Canadian Journal of Forest Research*, 39(1), 193–197.

1006 Rossini M, Meroni M, Migliavacca M, Manca G, Cogliati S, Busetto L, Picchi V, Cescatti A,

1007 Seufert G, Colombo R, (2010) High resolution field spectroscopy measurements for estimating

1008 gross ecosystem production in a rice field. *Agricultural and Forest Meteorology*, 150(9), 1283-

1009 1296.

1010 Rossini M, Nedbal L, Guanter L, Ač A, Alonso L, Burkart A, Cogliati S, Colombo R, Damm,

1011 A, Dusch M, Hanus J, Janoutova R, Julitta T, Kokkalis P, Moreno J, Novotny J, Panigada C,

1012 Pinto F, Schickling A, Schuttemeyer D, Zemek F, and Rascher U, (2015) Red and far red Sun-

1013 induced chlorophyll fluorescence as a measure of plant photosynthesis. *Geophysical Research*

1014 *Letters*, 42, 1632–1639.

1015 Rossini M, Meroni M, Celesti M, Cogliati S, Julitta, T, Panigada C, Rascher U, van der Tol C.

1016 and Colombo R, (2016) Analysis of Red and Far-Red Sun-Induced Chlorophyll Fluorescence

1017 and Their Ratio in Different Canopies Based on Observed and Modeled Data. *Remote Sensing*,

1018 8(5), 412.

1019 Rundel PW, & Yoder BJ, (1998). Ecophysiology of pinus. In Ecology and Biogeography of

1020 Pinus (ed. D.M. Richardson) pp. 296–323. Cambridge University Press, Cambridge, UK.

1021 Running SW, & Gower ST, (1991) FOREST-BGC, a general model of forest ecosystem

1022 processes for regional applications, II. Dynamic carbon allocation and nitrogen budgets. *Tree*

1023 *Physiol*., 9, 147-160.

1024 Ryan MG, Binkley D, Fownes JH, (1996) Age-related decline in forest productivity: pattern

1025 and process. *Adv. Ecol. Res*. 27, 213–262.

1026 Ryan MJ. & Yoder BJ, (1997) Hydraulic limits to tree height and tree growth. *Bioscience* 47,

1027 235−242

1028 Ryan MG, Binkley D, Fownes JH, Giardina CP, and Senock RS, (2004) An experimental test

1029 of the causes of forest growth decline with stand age. Ecological Monographs, 74(3), 393–414.

1030 Ryan MG, Phillips N, Bond BJ, (2006) The hydraulic limitation hypothesis revisited. *Plant Cell*

1031 *Environ* 29:367–381.

1032 Shirke PA, (2001) Leaf Photosynthesis, Dark Respiration and Fluorescence as Influenced by

1033 Leaf Age in an Evergreen Tree, Prosopis Juliflora. *Photosynthetica*, 39(2), 305–311.

1034 Sun Y, Fu R, Dickinson R, Joiner J, Frankenberg C, Gu L, Xia Y. and Fernando N, (2015)

1035 Drought onset mechanisms revealed by satellite solar-induced chlorophyll fluorescence:

1036 Insights from two contrasting extreme events. *J. Geophys. Res. Biogeosci*., 120, 2427–2440.

1037   Tasissa G, & Burkhart HE, (1998) Juvenile-mature wood demarcation in loblolly pine trees.

1038   *Wood and Fiber Science* 30(2), 119-127.

1039   van der Tol C, Verhoef W, Timmermans J, Verhoef A. and Su Z, (2009) An integrated model

1040   of soil - canopy spectral radiances, photosytesis, fluorescence, temperature and energy balance.

1041   *Biogeosciences* 6 (2009)12, 3109-3129.

1042   van der Tol C, Rossini M, Cogliati S, Verhoef W, Colombo R, Rascher U, Mohammed G,

1043   (2016) A model and measurement comparison of diurnal cycles of sun-induced chlorophyll

1044   fuorescence of crops. *Remote Sensing of Environment*, 186, 663-677.

1045   Van Wittenberghe S, Alonso L, Verrelst J, Hermans I, Delegido J, Veroustraete F, Valcke R,

1046   Moreno J. and Samson R, (2013) Upward and downward solar-induced chlorophyll

1047   fluorescence yield indices of four tree species as indicators of traffic pollution in Valencia.

1048   *Environmental Pollution*, 173, 29–37.

1049   Verhoef W, & Bach H, (2007) Coupled soil - leaf - canopy and atmosphere radiative transfer

1050   modeling to simulate hyperspectral multi - angular surface reflectance and TOA radiance data.

1051   *Remote sensing of environment*, 109(2), 166-182.

1052   Verrelst J, Rivera JP, van der Tol C, Magnani F, Mohammed G, and Moreno J, (2015) Global

1053   sensitivity analysis of the SCOPE model: What drives simulated canopy-leaving sun-induced

1054   fluorescence? *Remote Sensing of Environment*, 166, 8–21.

1055   Verrelst J, van der Tol C, Magnani F, Sabater N, Rivera JP, Mohammed G, and Moreno J,

1056   (2016) Evaluating the predictive power of sun-induced chlorophyll fluorescence to estimate net

1057   photosynthesis of vegetation canopies: A SCOPE modeling study. *Remote Sensing of*

1058   *Environment*, 176, 139–151.

1059 Walter-Shea EA, Privette J, Cornell D, Mesarch MA, Hays CJ, (1997) Relations between

1060 directional spectral vegetation indices and leaf area and absorbed radiation in alfalfa. *Remote*

1061 *Sensing of Environment*, 61, 162-177.

1062 Widlowski JL, (2010) On the bias of instantaneous FAPAR estimates in open-canopy forests.

1063 *Agricultural and Forest Meteorology*, 150, 1501-1522.

1064 Wieneke S, Ahrends H, Damm A, Pinto F, Stadler A, Rossini M, and Rascher U, (2016)

1065 Airborne based spectroscopy of red and far-red sun-induced chlorophyll fluorescence:

1066 Implications for improved estimates of gross primary productivity. *Remote Sensing of*

1067 *Environment*, 184, 654-667.

1068 Yoder BJ, Ryan MG, Waring RH, Schoettle AW and Kaufmann MR, (1994) Evidence of

1069 reduced photosynthetic rates in old trees. *Forest Science* 40, 513–527.

1070 Zarco-Tejada PJ, Miller JR, Harron J, Hu B, Noland TL, Goel N, *et al*., (2004) Needle

1071 chlorophyll content estimation through model inversion using hyperspectral data from boreal

1072 conifer forest canopies. *Remote Sensing of Environment*, 89, pp. 189–199.

1073 Zarco-Tejada PJ, González-Dugo V, and Berni JAJ, (2012) Fluorescence, temperature and

1074 narrow-band indices acquired from a UAV platform for water stress detection using a micro-

1075 hyperspectral imager and a thermal camera. *Remote Sensing of Environment*, 117, 322–337.

1076 Zarco-Tejada PJ, Suarez L, and Gonzalez-Dugo V, (2013) Spatial resolution effects on

1077 chlorophyll fluorescence retrieval in a heterogeneous canopy using hyperspectral imagery and

1078 radiative transfer simulation. *IEEE Geoscience and Remote Sensing Letters*, 10(4), 937–941.

1079 Zarco-Tejada PJ, González-Dugo MV, Fereres E, (2016) Seasonal stability of chlorophyll

1080 fluorescence quantified from airborne hyperspectral imagery as an indicator of net

1081 photosynthesis in the context of precision agriculture. *Remote Sensing of Environment*, 179,

1082 89–103.

1083 Zeide B, (1993) Analysis of growth equations. *Forest Science*, 39(3): 594-616.

1084 Zhang Q, Middleton EM, Cheng YB, Huemmrich KF, Cook BD, Corp LA, Kustas WP, Russ

1085 AL, Prueger JH, Yao T, (2016) Integrating Chlorophyll fapar and Nadir Photochemical

1086 Reflectance Index from EO-1/Hyperion to Predict Cornfield Daily Gross Primary Production.

1087 *Remote Sensing of Environment*, 186, 311–321.

1088 Zhang Y, Guanter L, Berry JA, Joiner J, van der Tol C, Huete A, Gitelson A, Voigt M, and

1089 Kohler P, (2014) Estimation of vegetation photosynthetic capacity from space-based

1090 measurements of chlorophyll fluorescence for terrestrial biosphere models. *Global Change*

1091 *Biology*, 20(12), 3727–3742.

1092 Zhao F, Dai X, Verhoef W, Guo Y, van der Tol C, Li Y, and Huang Y, (2016) FluorWPS: a

1093 Monte Carlo ray-tracing model to compute sun-induced chlorophyll fluorescence of three-

1094 dimensional canopy. *Remote Sensing of Environment*, 187, 385-399.